SYNTHESIS AND CHARACTERIZATION OF AMINE FUNCTIONALIZED ZIRCONIUM METAL ORGANIC FRAMEWORKS FOR PHOTOCATALYTIC DEGRADATION OF METHYL ORANGE

MSc THESIS

ADMASSU FELEKE BUBAMO

JUNE 2017

HARAMAYA UNIVERSITY, HARAMAYA

Synthesis and Characterization of Amine-Functionalized Zirconium Metal Organic Frameworks for Photocatalytic Degradation of Methyl Orange

A Thesis Submitted to the Department of Chemistry,
Postgraduate Program Directorate
HARAMAYA UNIVERSITY

In Partial Fulfillment of the Requirements for the Degree of
MASTER OF SCIENCE IN CHEMISTRY (INORGANIC CHEMISTRY)

Admassu Feleke Bubamo

June 2017
Haramaya University, Haramaya

HARAMAYA UNIVERSITY
POSTGRADUATE PROGRAM DIRECTORATE

We hereby certify that we have read and evaluated this Thesis titled *'Synthesis and Characterization of Amine-Functionalized Zirconium Metal-Organic Frameworks for Photocatalytic Degradation of Methyl Orange*' prepared under our guidance by Ademassu Feleke. We recommend that it can be submitted as fulfilling the thesis requirement.

Abi Taddesse (PhD)	_____	_____
Major Advisor	Signature	Date
Isabel Diaz (Prof.)	_____	_____
Co- Advisor	Signature	Date
Tesfahun Kebede (PhD)	_____	_____
Co- Advisor	Signature	Date

As members of the Board of Examiners of the MSc Thesis Open Defence Examination, we certify that we have read and evaluated the thesis prepared by Admassu Feleke and examined the candidate. We recommend that the thesis be accepted as fulfilling the Thesis requirement for the degree of *Master of Science in Chemistry* (Inorganic Chemistry).

_____	_____	_____
Chairperson	Signature	Date
_____	_____	_____
Internal Examiner	Signature	Date
_____	_____	_____
External Examiner	Signature	Date

DEDICATION

This thesis manuscript is dedicated to my wife Chako Teshome, Dr. Abi Taddesse and to all my family who encouraged, strengthened and for helping me with affection and love and for their dedicated partnership me in the success of my work.

STATEMENT OF THE AUTHOR

By my signature below, I declare and affirm that this Thesis is my own work. I have followed all ethical and principles of scholarship in the preparation and compilation of this Thesis manuscript. Any scholarly matter that is included in the Thesis has been given recognition through citation.

This Thesis is submitted in partial fulfilment of the requirements for MSc degree at the Haramaya University. The Thesis is deposited in the Haramaya University Library and is made available to borrowers under the rules of the Library. I solemnly declare that this manuscript has not been submitted to any other institution anywhere for the award of any academic degree, diploma, or certificate.

Brief quotations from this Thesis may be made without special permission provided that accurate and complete acknowledgement of the source is made. Requests for permission for extended quotations from or reproduction of this manuscript in whole or in part may be granted by the Head of the Department or Director of Postgraduate Program Directorate when in his or her judgment the proposed use of the material is in the interest of scholarship. In all other instances, however, permission must be obtained from the author of the Thesis.

Name: Admassu Feleke Bubamo Signature: _____

Date: _____

Department: Chemistry

BIOGRAPHICAL SKETCH

The author was born on the 23th of May 1986 at Gimbichu town. He attended his elementary and secondary education at various schools found in Soro Woreda, Hadiya Zone, South Nation Nationality People Region State. Later, he joined Awassa Teachers' Education College and graduated with Diploma in teaching chemistry in 2004. He was then assigned by the Educational Bureau of South Nation Nationality People Region State in Gimbichu Elementary School. After two years of service, he was transferred to Gimbichu Secondary and Preparatory School, where he served as a teacher, a unit leader, and department head and as Academic vice Director. Then he joined Haramaya University in 2006 in the summer program and received B.Ed. degree in chemistry in 2009. He continued his service for three years. He had been teaching in the Gimbichu secondary and preparatory school until he joined the Postgraduate Program at Haramaya University to pursue MSc program in Inorganic Chemistry in January 2014.

ACKNOWLEDGMENTS

First, I would like to thank the Almighty God for giving me abundantly life, health, strength, patience, understanding, and wisdom to withstand the inconveniences from the beginning to the completion of this work.

I would like to extend my sincere and heartfelt thanks to my major advisor Dr. Abi Taddesse, for his encouragement and genuine guidance from the very beginning of the selection of the research topic and providing me with the budget for the research work up to including forth thesis write up. Most importantly, he helped me in all synthesis and characterization. Truly speaking without his effort and contribution the completion of this work would not have been possible. I will always be indebted to him for all the knowledge he forced to know basic sciences and has shared with me.

I have my sincere thanks to my co-advisors, Dr. Tesfahun Kebede and Prof. Isabel Diaz, for their all rounded invaluable comments and professional advice from the early design of the proposal to characterization and the final write up of this thesis.

I am very thankful to the Institute of Catalysis and Petroleum Chemistry, for their great support to characterize the as synthesized MOF in Madrid, Spain. Also, I would like to thanks Mr. Zewdu Bezu, Dr. Yonas Chebude, Dr. Endale Taju and Mr. Fituma Diriba who give advice and assisted me during synthesis, visible degradation, PL and FTIR characterization and with some techniques during laboratory work.

The salary support I got from the Soro Woreda, which they jointly provided me with the opportunity to pursue my education and made this study possible is highly appreciated. Last but not least, I would like to thank my parents, family members and my friends for their unreserved encouragement and constant support.

ACRONYMS AND ABBREVIATIONS

BDC	1, 4-Benzenedicarboxylate/Terephthalate
BET	Brunauer, Emmett and Teller
DIW	Deionized Water

DMF	N, N-Dimethylformamide
FTIR	Fourier Transform Infrared Spectroscopy
H_2BDC	1, 4-Benzenedicarboxylic acid/Terephthalic acid
HPLC	High Pressure Liquid Chromatography
HT	High Temperature
MIL	Material Institute of Lavoisier
MO	Methyl Orange
MOF	Metal Organic Framework
PL	Photo Luminescence
PSM	Post-Synthetic Modification
PZC	Point of Zero Charge
NH_2-BDC	2-amino terephathalic acid
RS	Real Sample
RT	Room Temperature
SEM	Scanning Electron Microscopy
TEA	Triethylamine
TGA	Thermo Gravimetric Analysis
UiO	University of Oslo
UiO-66(Zr)	Zirconium 1, 4-benzenedicarboxylate MOF
UiO-66-NH_2 (Zr)	Zirconium-2-amino-1, 4-benzenedicarboxylate MOF
UV-Vis	Ultraviolet-Visible
XRD	X-Ray Diffraction

TABLE OF CONTENTS

Continued

Continued

LIST OF TABLE

Table
Page

LIST OF FIGURES

Continued

LIST OF TABLES IN THE APPENDIX

Appendix Table

Page

dark and visible light illumination (MO=10ppm, 0.3M H_2O_2 and 0.15gL^{-1} photocatalyst load with pH adjustment at 4).
77

Synthesis and Characterization of Amine-Functionalized Zirconium Metal-Organic Frameworks for Photocatalytic Degradation of Methyl Orange

ABSTRACT

The environmental pollution caused by any organic dye-containing wastewaters in textile, plastic, pulp, and paper industry is one of key problems. For this reason, UiO-66 and UiO-66- NH_2, photocatalysts were synthesized in different options by solvothermal and hydrot hermal method at Room Temperature and High Temperature condition to remove dyes from aqueous solution as well as real sample. Hence, Zirconium MOFs samples were synthesised successfully at Room Temperature and High Temperature with solvent Di-ionized Water and with DMF, respectively. Zr-MOFs samples were characterized for thermal stability, structure and crystallinity, topology, band gap energy, surface area and porosity, the presence of organic functional groups and optical intensity by TGA, XRD, SEM, UV-Vis, BET, FTIR and PL, respectively. The synthesized MOFs show, high thermal stability, excellent crystallinity, higher surface area, larger pore volume and less optical intensity. In this study, the effects of key parameters were examined to find out the optimum operating conditions of the photocatalytic degradation of methyl orange dye using Zr-MOFs under visible light radiation. The photocatalytic degradations of MO using all the as-synthesized photocatalysts were investigated under visible light irradiation. High performance of UiO-66-NH_2-DMF-TEA-HT towards degradation under visible light was observed. In effect, its lower PL intensity and the smaller band gap energy have enhanced the photocatalytic process by prolonging the

electron-hole recombination. In addition, amine-functionalized Zirconium MOFs have better degradation efficiency than non-functionalized MOFs. Moreover, UiO-66-NH_2-TEA can be easily regenerated and re-used for several times, which show this photocatalyst could have large potential for the degradation of dye-containing wastewater. Finally, the experimental results of selected MOFs were effective for the removal of MO aqua solution (88.93%) and real sample textile wastewater (71.24%).

***Keywords**: Adsorption, Metal organic frameworks, Methyl Orange, photocatalysis, and Photocatalytic degradation.*

1. INTRODUCTION

By definition, dyes can be said to be colored, ionizing and aromatic organic compounds which show an affinity towards the substrate to which it is being applied (Samar, 2015). Dyes are chemicals which on binding with a material gives color to the material .The color of the dye are provided by a chromophore group. A chromophore is a radical configuration consisting of conjugated double bonds containing delocalized electrons (Adeyamo *et al*., 2012). A dye is a colored substance that has an affinity to the substrate to which it is being applied. Dyes appear to be colored because they absorb some wavelengths of light more than others (Vakiti, 2012).
In due course of time, these synthetic dyes gained huge popularity and began to be synthesized on a large scale.

Although dyes make our world beautiful, they bring air/water pollution. Color is the first contaminant to be recognized in wastewater and has to be removed before discharging it into water bodies or onto land. The colored wastewaters of industrial effluents are unattractive because they account significant concentrations of pollutants so that they become the sources of increasingly acute complaints. They can have acute or chronic effects on exposed organisms, which depend on the concentration of the dye and the exposed time. In addition to that, many dyes are considered to be toxic and even carcinogenic (Rashed and El-Amin, 2007).

Efficient removal of organic pollutants from wastewater has become a hot research topic, due to its ecological and environmental importance. Industrial plants generate increasing amounts of wastewater, which causes severe environmental problems. Wastewater produced in many industrial processes contains organic compounds that are toxic and not amenable to direct

biological treatment. There are a huge number of different types of organic pollutants, including organic dyes, phenols, biphenyls, pesticides, fertilizers, hydrocarbons, plasticizers, detergents, oils, greases, pharmaceuticals, proteins, carbohydrates (Wang *et al*., 2014).

The presence of small amounts of dyes in water (even < 1 ppm) is highly visible and it affects the pleasant appearance, causes significant loss in luminosity and any increase in the temperature will greatly deplete the dissolved oxygen concentration in wastewater. This results in subsequent alteration of the aquatic ecosystem (Vakiti, 2012). Thus, the presence of dye materials greatly influences the quality of water and the removal of this kind of pollutant is of prime importance (Agarwal, 2013).

Conventional dye removal methods, including physical, chemical, and biological processes, have been used intensively as a solution for the problem. But these methods have disadvantages such as impacts on health, high cost and difficulty in recycling. It is also a problem because these dye compounds in wastewater ordinarily contain one or several benzene rings and cannot be decomposed easily in chemical and biological processes. Moreover, most of the dyes are found to be resistant to normal treatment process as they are designed to resist chemical and photochemical degradation (Mohanty, 2012).

But porous solids based heterogeneous photocatalytic technology was developed as a promising solution to this challenge. MOFs behave as semiconductors when exposed to light, thus making MOFs potentially be photocatalysts. More recently, MOFs that can act as photocatalysts have attracted much attention for exploiting new applications of MOFs (Du *et al*., 2011).

Metal-organic frameworks (MOFs) are coordination polymers formed by linking inorganic and organic units by strong bonds (Furukawa *et al*., 2013). They exhibit high surface areas and large pore volumes attracting considerable attention, due to their well-designed topology and potential applications in gas separation, gas storage, thermal expansion, molecular sensing, ion exchange, and catalysis.

Recently, researchers have started to investigate the capability of MOFs as adsorbents in the wastewater treatment. It is found that several types of MOFs are stable in water and exhibit promising adsorption capacities for the removal of pollutants from water such as metal ions (Ke *et al*., 2011), toxic dyes (Li *et al*., 2013), and organic dyes (Lin and Chang, 2015). Some

MOFs reveal even higher adsorption capacities than conventional adsorbents, like granular activated carbon (Khan *et al*., 2015).

The post-synthetic modification (PSM) of MOFs is a viable route for synthesizing functionalized MOFs and generating multiple active sites (Nguyen and Cohen, 2010; Hou *et al*., 2015). Recently, MOFs have attracted attention as catalysts in the degradation of dyes under visible irradiation owing to their high surface area, low densities, and high porosity, thermal stability and adjustable chemical functionalities (Mohanty, 2012).

Zirconium and titanium based MOFs exhibit exceptional stability in aqueous solution. However, both zirconium (UiO-66) and titanium (MIL-125)-based MOFs belong to a wide band semiconductors limited only to UV portion of the solar spectrum. Recently, amine functionalized MOFs of zirconium (UiO-66-NH_2) and titanium (MIL-125-NH_2) have evidenced a red shift in the UV-Vis absorption spectrum compared with the un-functionalized congeners and some literatures proved the visible photocatalytic activities of these compounds (Lin *et al*., 2015).

However, there is still a dearth of information in terms of facile synthesis of these compounds. There has been only little reports by (Haque *et al*., 2010; Kandiah *et al*., 2010; Du *et al*., 2011; Adeyemo *et al*., 2012; Long *et al*., 2012; Agarwal, 2013; Negash, 2013; Shen *et al*., 2014; Khan *et al*., 2015; Lin and Chang, 2015; Lin *et al*., 2015) on the use of MOFs in the removal of dye materials while MOFs have certainly attracted increasing interest due to their rich structural chemistry and tuneable physical properties.

Therefore, the main aim of this study is to synthesize UiO-66 and UiO-66-NH_2 MOFs both at room temperature in distilled water and using DMF as a solvent at relatively high temperature. Generally, there has been a research gap on the options/ facile synthesis, characterization and evaluation of the photocatalytic activity of amine-functionalized zirconium MOFs for the efficient removal of dye materials.

General objective:

- The overall objective of the study is to synthesize and characterize amine-functionalized zirconium MOFs for photocatalytic degradation of MO dye from aqueous solution and real sample collected from textile effluents under visible irradiation.

Specific objectives:

- To synthesis both UiO-66 and UiO-66-NH_2 MOFs at room temperature and at higher temperature in different options.
- To characterize the as-synthesized MOFs using XRD, TGA, FTIR, PL UV-Vis, BET, and SEM.
- To study the photocatalytic degradation of MO using as-synthesized MOFs under visible irradiation.
- To compare the photocatalytic effect of UiO-66 and UiO-66-NH_2 under visible irradiation.
- To employ the as-synthesized MOFs for textile wastewater treatment application.

2. LITERATURE REVIEW

2.1. Photocatalysis

In chemistry, photocatalysis is the acceleration of a photoreaction in the presence of a catalyst. In catalyzed photolysis, light is absorbed by an adsorbed substrate. In photo generated catalysis, the photocatalytic activity (PCA) depends on the ability of the catalyst to create electron–hole pairs, which generate free radicals (e.g. hydroxyl radicals: •OH) able to undergo secondary reactions. The commercially used process is called the advanced oxidation process (AOP**).** Photocatalysis is one of the advanced oxidation processes (AOPs) that has attracted considerable attention to researchers, due to the fact that they can effectively remove environment pollution under UV and/or visible light (Jiang *et al*., 2012; Habeeb *et al*., 2016).

2.2. Organic Dyes

Dyes are chemicals, which on binding with a material which give color to them. Dyes are ionic, aromatic organic compounds with structures including aryl rings, which have delocalized electron systems. The color of dye is provided by the presence of a chromospheres group. Synthetic organic dyes have been widely used for dying textile fibers such as cotton and polyesters (Adeyemo *et al.,* 2012). Dyes stuffs are characterized in accordance with their capacity to absorb the energy of a particular part of the electromagnetic radiation to which the human eye is sensitive.

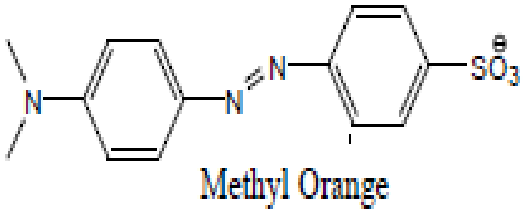

Figure 1. The chemical structures of MO

Methyl orange is one of the well-known acidic/anionic dyes, and has been widely used in textile, printing, paper, food and pharmaceutical industries and research laboratories (Mittal *et al*., 2007). For this reason, MO was selected in this study.

2.3. Dyes Adsorption

Adsorption is the attachment of molecules (adsorbate) to a surface; the surface is also known as an adsorbent (Mohamed, 2011). It is based on the capability of porous materials with large surfaces to selectively retain compounds on the surface of the solid (adsorbent). The adsorbent may be any material that provides surface area with adsorption sites for attachment of molecules or particles (Adeyamo *et al*., 2012). Organic pollutants such as organic dyes in waste water, with high toxicity and hard degradation, have become one of the most serious environmental issues today (Tsai, 2007; Tsai *et al*., 2014). Recently, MOFs with the abilities of absorption and separation of pollutants have been applied in related fields. However, only a few MOFs have been used to absorb or separate dye molecules. Taking into account the stability and low toxicity of Zirconium based MOFs; they should be suitable as dyes delivery agents (Wang *et al*., 2014). Adding functional group in structures is one of the methods to increase the adsorption capacity and photocatalytic performance of MOFs (Luu *et al*., 2015).

2.4. Organic Dye Effluent Treatment Methods

Effluents from textile industries are the most expressive from an ecological and physiological perspective (Mohanty, 2012; Agarwal, 2013). In order to achieve satisfactory and acceptable quality levels treatment methods that allow recycling of textile wastewater, removal of dyes and related compounds are very crucial. Based on the fact that dyes constitute the large percentage of textile wastewater, most treatment methods are based on the decolorization (Haque *et al*., 2010; Laurier *et al*., 2013).

Synthetic organic dyes have been widely used for dyeing textile fibers such as cotton and polyesters (Adeyemo *et al*., 2012). Recently, considerable amount of wastewater with color has been generated from many industries including textile, leather, paper, printing, and dyestuffs, plastic and so on (Crini, 2006). Textile industries consume large volumes of water and chemicals during wet processing stages (Pelizzetti, 1985). The removal of dye materials from water is very important because water quality is highly influenced by color and even a small amount of dye is highly visible and considered to be toxic and extremely hazardous to aquatic living organisms (Mohanty et al., 2012).

It is difficult to degrade dye materials because they are very stable to light and oxidation reactions (Mittal *et al*., 2007). For the removal of dye materials from contaminated water, several methods such as physical, chemical and biological methods have been investigated (Mittal *et al*., 2007; Mohanty, 2012). Each dye removal technique has its limitations and one individual process may not be sufficient to achieve complete decolorization. To overcome this problem, dye removal strategies involve a combination of different techniques (Sadri, 2010).
Among the suggested methods, removal of dyes by adsorption technologies is regarded as one of the competitive methods, because of its high efficiency, economic feasibility and simplicity of operation (Mittal *et al*., 2007). In addition, photocatalytic H_2 generation from water by using solar energy provides an environmentally benign way, but the key is to develop highly active and stable photocatalysts at low cost (Long *et al*., 2006; Shen *et al*., 2014).

2.5. Metal Organic Frameworks

2.5.1 Definition of MOFs

Metal-organic frameworks (MOFs) are coordination polymers formed by linking inorganic and organic units by strong bonds (Furukawa *et al*., 2013). Metal organic frameworks are highly crystalline materials built from inorganic and organic building blocks with infinite inorganic-organic connectivity, forming soluble complexes that then self-assemble into one-, two-, or three-dimensional frameworks consisting of metal ions linked together by organic bridging ligands. Sometimes they are referred to as hybrid inorganic-organic frameworks and a subset of which are inorganic coordination polymers (Wilkinson *et al*., 1987).

2.5.2. Structural Composition of MOFs

A metal-organic framework (MOF) material can be thought of as the composition of two major components: a metal ion and an organic molecule called a linker (James, 2006). These organic molecules act as a linker to link the metal ions. The backbone of the compound is constructed from metal ions which act as connectors and organic bridging ligands as linkers (Adedibu and Isaac, 2012).

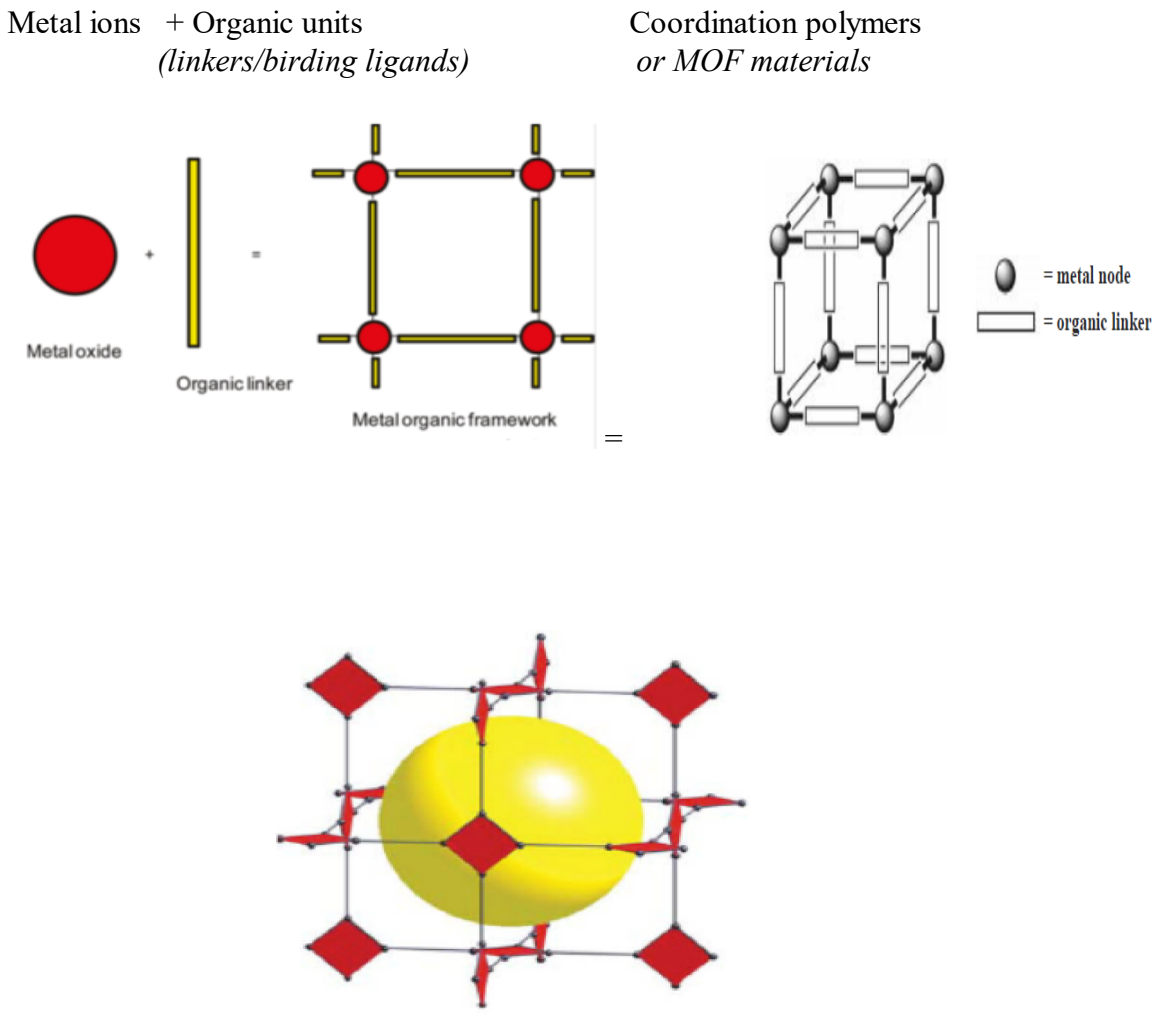

Figure 2.Schematic representation of a MOF unit cell showing the arrangement of metal ions and inorganic joints (*Ma., 2011*).

The organic ligands or linkers are groups that can donate multiple lone pairs of electrons (polydendate) to the metal ions, whereas the metal ions are made up with vacant orbital shells that can accept these lone pairs of electrons to form metal-organic framework materials.

2.5.3. Post Synthetic Modification (Functionalization) of MOFs

The functionalization of MOF materials (PSM) is a powerful strategy to tune their properties of porous materials to fit practical applications (Almansa, 2016). MOFs can be easily modified by post-synthesis treatments with the aim of introducing functional groups that can act or be transformed into catalytic active sites (Tanabe and Cohen, 2011). Metal-organic frameworks (MOFs) are usually obtained from a ‘‘one pot’’ synthesis where there is no opportunity available for the adjustment of the properties during the formation of the material (Wang and Cohen, 2009). Therefore, functionalized networks can be prepared by undertaking reactions on preformed MOFs. The pore architecture of the preformed MOF can be tailored by PSM for a specific purpose in order to tune the material for selective adsorption and catalysis (Tanabe and Cohen, 2011). Therefore, PSM can be defined as chemical derivatization of MOFs after their formation (Kandiah *et al*., 2010).

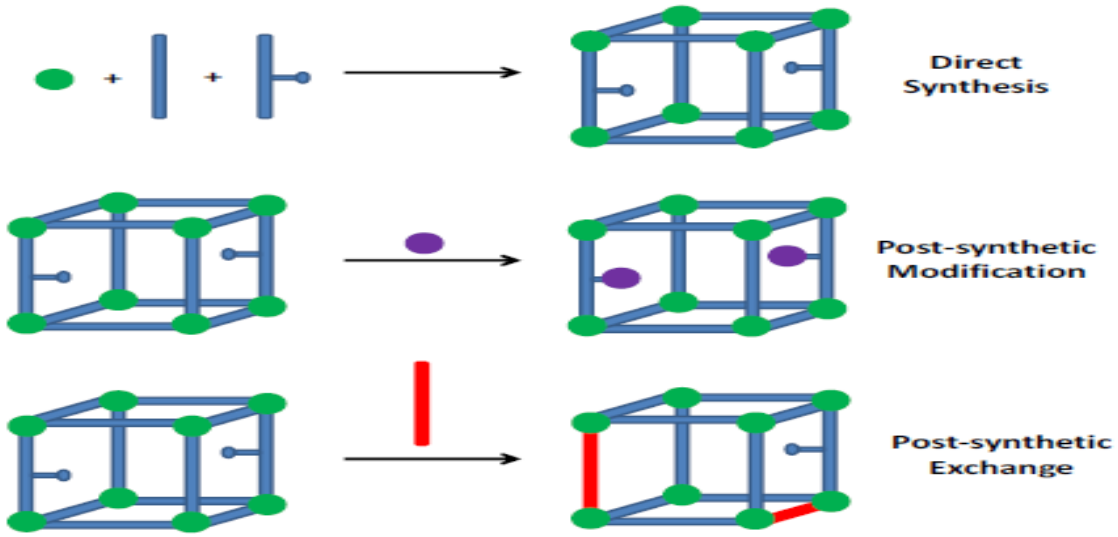

Figure 3. A generic scheme for the post synthetic modification (PSM) of MOFs
(Almansa, 2016)

2.5.4. Morphology of MOFs

The topologies of MOFs structure is determined by the coordination geometry of both the metal nodes (metal ions or metal-carboxylate SBUs) and the organic linkers. The bonds formed between the metal ions and the donor atoms of the linker are strong and, as a result, the extended network structure in the MOF is quite robust. The coordination complex formed by the metal ions and the donor atoms of the linker, also termed the secondary building unit (SBU), dictates the final topology of the MOF framework (Stock and Biswas, 2012). The properties of resulting frameworks, like pore diameter, pore structure, and structure porosity, are thus different. The metal nodes control the extension geometry and the organic linkers control features such as the binding strength, the directionality of propagation and size of the pores formed in such materials. MOFs are over ninety percent empty space and yet still incredibly strong and flexible and can be simply and controllably customized at a molecular level for specific applications. This may sound like the stuff of science fiction. However these

materials, called metal-organic frameworks or MOFs, are now a reality and are set to play a significant role in several key technology areas (Long *et al*., 2006).

2.5.5. Properties of MOFs

MOFs are well-defined, adjustable and highly porous materials with spatial confinement, often crystalline, sensitive to air and resistant to structural collapse upon heating (James *et al*., 2006). They have unique properties, such as highly diversified structure, large range in pore sizes, high surface areas, and specific adsorption affinity. The most intriguing characteristic of MOFs is their exceptional specific surface area. The unprecedentedly high surface areas of MOFs make them stand out from other porous materials, and the nano space inside their frameworks allows them to efficiently trap various gas molecules. Unlike other porous materials, MOFs are open scaffolds that have pores without walls, a feature that endows these materials with exceptionally large surface areas. In addition, since the topology of the scaffold is defined by molecular building blocks, the pore or aperture size within the framework is quite small, typically less than 20 Å, leading to strong interactions between guest molecules and the framework. The porosity of MOFs is greater than that of any other porous material, including activated carbons, making MOFs ideal candidates for use as adsorbents (James**,** 2003; Adedibu and Isaac, 2012). Due to their structural and functional tenability, the area of MOFs has become one of the fastest growing fields in chemistry (Susuma and Joe, 2014).

2.5.6. Amine-functionalized Zirconium MOFs

Among the large family of metal-organic frameworks, Zr-based MOFs, which exhibit rich structure types, outstanding stability, intriguing properties and functions, are foreseen as one of the most promising MOF materials for practical applications. As literature reports have previously mentioned, the Zr-MOFs consist of a Zr (IV)-carboxylate cluster Zr_6 (μ_3-O)$_4$(μ_3-OH) $_4(CO_2)_{12}$, which works as the inorganic secondary building unit for the framework (Almansa, 2016).

Zirconium (IV)--based MOFs (UiO-66) are selected in particular because of their exceptional high thermal and chemical stability (Kandiah *et al*., 2010; Almansa, 2016). Since MOFs can be functionalized by selecting different ligands, the effect of amine functional groups, which have been reported to enhance phosphate adsorption (Hamoudi *et al*., 2010).

Long *et al*. (2012) report an amine-functionalized zirconium MOF (UiO-66-NH_2) that under ≥ 420 nm light (here after, light) irradiation catalyzes the aerobic oxygenation of a wide range of organic compounds including alcohols, olefins and cyclic alkanes at high efficiency and high selectivity. UV-Vis diffuse reflectance spectra (DRS) show the photo absorption edge of UiO-66 could be shifted to the visible light region by simply introducing the amino group (-NH_2) on the organic ligand (Lin *et al*., 2015). In addition, its band gap energy of 2.75 eV has been reported depending on relation of Eg = 1240/λ (Long *et al*., 2012; Musho *et al*., 2014). Recently, some of the amino derivatives of MOFs were used for the adsorption of chemicals in different media and it has been found that –NH_2 can promote the electrostatic interaction between MOFs and a substrate (Chen *et al*., 2015). Furthermore, owing to the individual micro-pore structure of UiO-66-NH_2 and its negative zeta potential resulted from the charge balance for the protonation of -NH_2, UiO-66-NH_2 displays much higher adsorption capacity for cationic dyes and lower adsorption capacity for anionic dyes than UiO-66 (Chen *et al*., 2015). The porosity of UiO-66 (0.48cm^3/g) was greater than that of UiO-66-NH_2 (0.45cm^3/g). Moreover, the surface area of UiO-66-NH_2 (1023m^2/g) was lower than that of UiO-66 (1188m^2/g) (Shen *et al*., 2014; Lin *et al*., 2016).

2.6. Synthesis Methods of MOFs

There are several synthesis methods of MOFs developed throughout the years. The most commonly used include hydro- or solvothermal synthesis under conventional oven, microwave irradiation, electrochemical synthesis, ionothermal synthesis, sonochemical synthesis, mechanochemical synthesis, room temperature synthesis, and so on. Some reaction parameters are needed to be considered in order to reproduce the MOF materials. These are composition of the reactants, pH of the reaction medium, reaction temperatures, reaction time, and solubility of the reactants, solvent type, and concentration of the reactants, heating and cooling rates and types of reaction container (Vakiti, 2012; Chen *et al.,* 2012).

2.6.1. Hydro- and Solvo-thermal Synthesis

Hydro- and solvothermal synthesis are the most common methods used for making MOFs. Hydrothermal synthesis involves water as the solvent whereas solvothermal refers to the use of

organic solvents. The choice of solvent is based on its ability to dissolve the organic linker. In both cases, the reactions take place inside a Teflon-lined stainless steel autoclave. Since it is a closed system, an autogenous pressure will be built up**.** The reaction mixture is normally heated at temperatures ranging from 80 to 220^{o}C, over a time of several hours to several days. Compared with microwave, electrochemical and mechanochemical techniques, the use of autoclaves is a slow method (Yaghi and Li, 1995; Mikaela, 2012; Vakiti, 2012).

2.6.2. Ionothermal Synthesis

Ionothermal synthesis involves the use of, as the name implies, ionic liquid, which act as the solvent. Ionic liquids have many attractive properties and have been used for producing many new structures. Their high polarity and pre-organized structure give them excellent solvating abilities. They are suitable for high temperature reactions, as in autoclaves and microwave ovens, since they have high thermal stability and possess little measurable vapour pressure (James *et al.,* 2006).

2.6.3. Microwave Synthesis

Microwave-assisted synthesis can be applied for making MOFs to reduce the reaction time and/or heating temperature and increase the purity of the product. Microwave synthesis in organic chemistry has attracted considerable attention over the last decade as a result of its short reaction times. Microwave synthesis was extended to the synthesis of zeolites and more recently has been applied for the production of MOFs. It was not until recently that this method was applied to the synthesis of MOFs. Fast reaction rates, high yields and selectivity, low amounts of waste and the possibility to control the size, shape and quality of the crystals are the main advantages of microwave synthesis. The fast reaction times achieved with microwave heating can be explained by the increased number of nucleation sites due to the rapid heating. The particle size generally decreases using microwave heating compared with conventional methods (Mikaela, 2012; Stock and Biswas, 2012).

2.6.4. Mechanochemical Synthesis

Mechanochemical synthesis can work in the absence of solvents. Solvents are nearly always added to reactions to facilitate the diffusion and collision of the components. However, solvent is not always necessary. The metal salt and the acid, both solids, were ground using a ball mill without any addition of solvent or heat. The reaction was initiated by minimizing the particle

size, which facilitate the interaction between the metal salt and the acid. The reaction is accelerated by further grinding (James *et al.,* 2006).

2.6.5. Room Temperature Synthesis

In this method the metal salt solution in a specific solvent and the linker solution in the same/different solvent are prepared and mixed with stirring. The resultant solution is further stirred for longer hours on a magnetic stirrer and the product is separated by filtration, washed several times with the solvent and dried at room temperature (Yaghi *et al*., 2008; Negash, 2013; Manuel *et al*., 2014; Negash *et al*., 2014).

2.7. Characterization Techniques of MOFs

There are different techniques to characterize the as-synthesized crystalline MOF materials. The basic techniques are discussed below:

2.7.1. Fourier Transform Infrared Spectroscopy

Fourier transform infrared spectroscopy is one of the most common spectroscopic techniques used by organic and inorganic chemists. Infrared radiation is passed through the sample and a detector measures the energy of the transmitted radiation. Examination of this transmitted light shows how much energy has been absorbed at each wavelength. FTIR is used here to determine the types of functional groups present in the MOFs (Shen *et al*., 2014).

2.7.2. Photoluminescence Study

Photoluminescence (PL) spectroscopy is a non-destructive analytical technique in which a material is illuminated with light, usually from a laser, and the resulting luminescence is recorded as a plot of emitted light intensity versus wavelength (Jiao *et al*., 2012). It is light emission from any form of matter after the absorption of photons (electromagnetic radiation). Following excitation various relaxation processes typically occur in which other photons are re-radiated. Time periods between absorption and emission may vary by ranging from short fem to second-regime for emission involving free-carrier plasma in inorganic semiconductors (Hayes and Deveaud, 2002) up to milliseconds for phosphorescent processes in molecular systems; and under special circumstances delay of emission may even span to minutes or hours. Photoluminescence can provide information for characterization of the optical and electronic properties of semiconductors and molecules (Tuschel, 2016)

2.7.3. X-Ray Diffraction

X-ray diffraction (XRD) is a non-destructive analytical technique that can be applied for the identification of unknown specimens and for the determination of materials properties. It is the most important and beneficial technique in solid state chemistry and it has been applied for the fingerprint characterization of crystals and for the determination of their structures. This method requires an X-ray source (monochromatic or of variable wavelength), the sample which is under investigation and a detector that takes the diffracted X-rays (Ece, 2012).

2.7.4. Thermo gravimetric Analysis

Thermo gravimetric analysis (TGA) measures the mass change in a sample as a function of temperature or time, under a controlled atmosphere. It is widely used for porous material characterization and it provides a quantitative measurement of the mass changes in a material associated with both material transitions and thermal degradation and thus can be used in the determination of the thermal stability and decomposition products of a material and results are given as a continuous chart record (Negash, 2013).

2.7.5. Scanning Electron Microscopy

Scanning electron microscopy (SEM) is a powerful technique in the examination of materials surface morphology. SEM uses a focused beam of high energy electrons to scan the surface of a solid specimen. The electrons interact with the atoms at the surface, from a region about 2 microns in depth, producing signals which create an image for the analysis of the secondary and backscattered electrons. The interactions between the electrons and the sample give information regarding morphology of the as-synthesized sample (Gu, 2014).

2.7.6. N_2 Adsorption and Brunauer, Emmett and Teller

BET theory explains the adsorption of gas molecules on solid surfaces. It serves as the basis for the measurement of specific surface area of a material .Porous solids are classified as microporous, mesoporous and macroporous based on the size of their pores. Solids which have a pore size of 2 nm or below are known as microporous. The mesoporous solids are in the range of between 2 nm and 50 nm and above 50 nm are known as macroporous (Negash, 2013). Depending on the amount of gas adsorbed, the resultant sample pressure is recorded. From this the surface area can be calculated (Mohanty, 2012).

2.8. The Chemistry and Applications of MOFs

Unlike other extended solids, MOFs maintain their underlying structure and crystalline order upon expansion of organic linkers and inorganic secondary building units, as well as after adjustable chemical functionalization, which greatly widens the scope of this chemistry (Furukawa *et al*., 2013). Careful selection of MOF constituents can yield crystals of ultrahigh porosity, high thermal and chemical stability; high surface areas and void volumes. The precision commonly exercised in their chemical modification and the ability to expand their metrics without changing the underlying topology has not been achieved with other solids. Due to these reasons MOFs have applications in many areas of chemistry and biochemistry, including gas separations, drug delivery, ion exchange, molecular storage, gas storage, sensing and catalysis (Achmann *et al*., 2009; Alemseged *et al.,* 2013; Furukawa *et al*., 2013). The following are some applications of MOFs:

2.8.1. Gas Separation

The most notable study of MOFs as loading materials is the storage of fuel gas H_2/CH_4 and greenhouse gas CO_2 (Ma, 2011). Adsorption processes and membrane separations are two dominant technologies that have been applied in industrial waste treatment. Commercial available meso- and macro-porous activated 12 carbons have been applied to waste water treatment system in order to remove contaminants e.g. heavy metal ions, dye, and organic molecules. Metal organic frameworks also show their potential application in flue gas treatment such as CO_2 (Holliday and Smith, 2014).

2.8.2. Drug Delivery

There is a strong interest in the development of methods for the controlled drug release to deliver the entire dose needed over a prolonged time with only one administration (Kuppler, 2009; Pham, 2013; Holliday and Smith, 2014). The regular porosity and the presence of organic groups within the framework of MOFs, combined with the low toxicity of carboxylic acids and some transition metals (Fe, Zn, Ti, Zr...), makes them attractive candidates for the controlled release of drugs. Taking into account it is a non-toxic material; MOFs can be altered for limitless applications in biomedicine in the future (Pham, 2013).

2.8.3. MOFs as Adsorbents for Synthetic Dye Removal

The difficulty encountered in degrading dye materials because they are very stable to light and oxidation reactions has formed the basis for the search of adsorbents suitable to remove dyes from contaminated water (Chen *et al*., 2010). The adsorption capacities of this MOF were much higher than the commercially available activated carbon. Thus, MOF-type materials were suggested as potential adsorbents in removing harmful materials (dyes inclusive) in the liquid phase (Haque *et al*., 2011).

Optimizing the pore surface, either using customized metal nodes and organic linkers with functionality already present or by post-synthetic covalent organic linkers with modification, aiming at controlling the adsorbate framework interaction is another way to facilitate selective molecule adsorption/separation (Adedibu and Isaac, 2012; Andrew *et al*., 2013).

2.8.4. Clean Energy Storage

Energy is an important part of our daily life. Cars and other internal combustion engines need the energy from fossil fuel to function. However, fossil fuel leads to some environmental problems, for instance acid rain, stratospheric ozone depletion, development of the greenhouse effect and air pollution. These environmental problems also have a negative effect on public health. Furthermore, the supply of oil is limited and supplies are likely to become scarce in the foreseeable future. As a result, a number of solutions have been proposed (Kuppler, 2009; Ma and Zhou, 2010; Ma and Meng, 2011; Holliday and Smith, 2014).

2.8.5. MOFs as Luminescence and Sensors

The potential use of MOFs as luminescent materials has spurred much interest in the area. Many gas detectors developed for portable applications are based on the change in electric resistivity with varying gas concentration and the sensitivity is normally dependent on surface area (Kuppler, 2009; Hinterholzinger, 2013). Therefore, nanoparticle metal oxides and porous materials with large specific surface areas, and high sensitivity to slight changes in environments (temperature, atmosphere, humidity, and light) are being developed and applied as detectors of combustible gases, humidity, ethanol, and hydrocarbons. Recent studies revealed that metal organic frameworks have the potential for sensor application (Achmann *et al*., 2009). The MOFs that possess luminescent properties together with size- or shape-selective sorption properties can be used as sensing devices (Adedibu and Isaac, 2012).

2.8.6. MOFs as Heterogeneous Photocatalysts

Photocatalysis is a proven, useful approach to solve environmental issues such as air and water pollution. Photocatalytic degradation of organic compounds is the most unexplored area in MOF photocatalysis (Du *et al*., 2011; Chen and Qian, 2014). MOFs behave as semiconductors when exposed to light, thus making them potentially be photocatalysts. More recently, MOFs that can act as a photocatalysts have attracted much attention for exploiting new applications of MOFs (Du *et al*., 2011).

In heterogeneous catalysis, the catalyst and the substrate(s) are in different phases. Most often, the catalyst is solid and the reactants are dissolved in a liquid phase or in a gas phase. The handling of a heterogeneous catalyst is usually easier than that of a homogeneous one. The reason is that a heterogeneous catalyst is insoluble in the reaction mixture and can therefore, easily be removed by filtration, recovered and be further reused in multiple cycles (Ma, 2011; Mikaela, 2012).

The following few reports also show that MOFs have heterogeneous photocatalytic activity for organic pollutant removal from aqueous solution. Actually, several studies that demonstrate the successful applications of MOFs in photocatalysis, mostly for photocatalytic dye degradation or hydrogen production, have emerged. As photocatalysts, MOFs are superior to semiconductors, since their light absorption ability can be more easily tuned by modifications on the metal ions and the organic linkers to achieve an efficient utilization of solar energy. Recently, by facile ligand substitutions, the researcher successfully obtained NH_2-MIL- 125 (Ti) and NH_2-UiO-66 (Zr), which are active in photocatalytic CO_2 reduction under visible light irradiation (Almansa, 2016). An amine-functionalized zirconium metal–organic framework (MOF) was used as a visible-light photocatalyst for selective aerobic oxygenation of various organic compounds including alcohols, olefins and cyclic alkanes, at high efficiency and high selectivity (Long *et al*., 2012).

Metal-organic frameworks contain in their structure light-absorbing organic chromophore and photo excitable semiconductor metal nodes. Moreover, a charge-transfer interaction between the organic moiety as donor and the metal cluster as acceptor is responsible for the extended absorption at longer wavelengths than those of the organic and inorganic components independently. Therefore, these materials combine properties typical of semiconductor quantum

dots with those conferred by the organic spacer. The organic molecule can act as a photon antenna for light harvesting, photosensitizing by energy transfer or electron injection the metal quantum dot that ultimately will be responsible for the photocatalytic activity (Francesc *et al*., 2007). In principle, MOFs can be synthesized in a systematic route to functionalize their structures (Schroder, 2010).

2.9. Mechanism for Degradation of Dyes

Generally, there are four essential key steps in the mechanism of heterogeneous photocatalysis on the surface of semiconductor (Mohamed, 2011), as follows:(1) charge carriers generation, (2) charge carriers trapping, (3) charge carriers recombination and (4) photocatalytic degradation of organic pollutants.

Upon irradiation with suitable light energy the electron from the valence band of the MOF catalysts promoted to its conduction band creating holes in valence band and electrons in conduction band. The electrons on the conduction band of the MOF catalyst surface are scavenged by the molecular oxygen to produce reactive oxygen radicals, whereas the holes in the valence band become trapped by the surface bound hydroxyl radicals that at produced on oxidation of either the surface hydroxyl group and/or the surface bound water molecules. These hydroxyl radicals have very high oxidation potential, hence named advanced oxidation process (AOP), which results in the oxidation of the pollutants (Herrmann *et al*., 1999). Hence, the oxidation of the pollutants results to simple harmless end products such as carbon dioxide, water and inorganic salts (Du *et al*., 2011; Samar, 2015). The overall basic mechanism of relevant reactions at the semiconductor surface causing the degradation of dyes can be expressed as follows (Colmenars and Luque, 2014).

$$\text{MOF (semiconductor)} + h\nu/\text{UV} \rightarrow \text{MOF } (e^-(\text{CB}) + h^+ (\text{VB}) \quad (1)$$

$$\text{MOF } (h^+_{VB}) + H_2O \rightarrow \text{MOF} + H^+ + OH^- \quad (2)$$

$$\text{MOF } (h^+_{VB}) + OH^- \rightarrow \text{MOF} + OH\bullet \quad (3)$$

$$MOF\ (e^-_{CB}) + O_2 \rightarrow O_2^{-\bullet} \quad (4)$$

$$O_2^{-\bullet} + H^+ \rightarrow HO_2^{\bullet} \quad (5)$$

$$HOO^{\cdot} + e^- \rightarrow HO_2^- \quad (6)$$

$$HOO^- + H^+ \rightarrow H_2O_2 \quad (7)$$

$$H_2O_2 + e^- \rightarrow OH^{\bullet} + OH^- \quad (8)$$

$$Dye + OH^{\bullet} \rightarrow \text{degradation products} \quad (9)$$

$$Dye + h^+_{VB} \rightarrow \text{oxidation products} \quad (10)$$

$$Dye + e^-_{CB} \rightarrow \text{reduction products} \quad (11)$$

Organic waste (dye) ⇒ photocatalyst/O_2/ $hv \geq E_g$ ⇒ dye + O_2 +OH• (Intermediates) ⇒

$$\rightarrow CO_2 + H_2O + \text{other products} \quad (12)$$

Where *hv* is photon energy required to excite the semiconductor electron from the valence band (VB) region to conduction band (CB) region

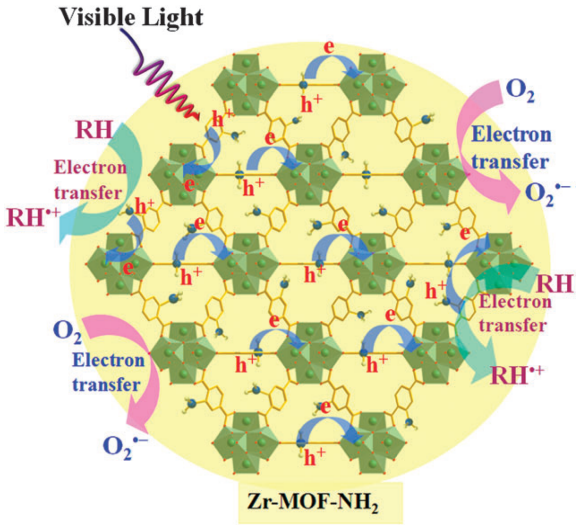

Figure 4. Photocatalytic mechanism of UiO-66-NH_2 (Long *et al*., 2012)

2.10. Factors Affecting Photocatalytic Process

There are several steps required for carrying out the process of photocatalytic degradation and those steps have the potential to limit the rate of pollutant degradation. Therefore, it is obvious that operational parameters related to each of these agents may affect the efficiency of the photocatalytic process. Photocatalytic reaction rates are known to be affected by several operation conditions including catalyst loading, pH of the medium, the surface charge of photocatalyst, initial dye concentration, and intensity of light, electron acceptors, electron scavengers, and temperature and oxygen pressure. Also, physical and chemical intrinsic properties of the photocatalyst may affect its photo efficiency (Chong *et al*., 2010).

2.10.1. Effect of Photocatalyst Load

The initial rates of reaction are directly proportional to the mass (m) of catalyst. However, above a certain value of m, the reaction rate levels off and becomes independent of mass (Shankar *et al*., 2004). The increase in the efficiency seems to be due to the increase in the total surface area (active sites) available for the photocatalytic reaction as the dosage of photocatalyst increased. However, when catalyst was overdosed, the number of active sites on the catalyst surface may become almost constant because of the decreased light penetration *via* shielding effect of the suspended particles and the loss in surface area caused by agglomeration (Sobczynski *et al*., 2004).

2.10.2. Effect of Initial Dye Concentration

As the concentration of model pollutant increases, more molecules get adsorbed on the

photocatalyst surface, the substrate concentration can influence the extent of adsorption and rate of reaction at the surface of the photocatalyst. It will be an important parameter for optimization between high degradation rate and efficiency. Mahalakshmi *et al*. (2009) found the optimum concentration for the dye under investigation and the rate increases up to this point but above this concentration, the rate decreases due to insufficient quantity of •OH radicals, as the formation of •OH radicals is constant for a given amount of the catalyst. Similarly, Zhu *et al*. (2000) reported that the photo generation of holes or ·OH radicals on the catalyst surface is reduced since the active sites are covered by dye ions. Another possible cause is the radiation screening effect at a high dye concentration since a significant amount of radiation may be absorbed by the dye molecules rather than the photocatalyst particles and then reduces the efficiency of the catalytic reaction (Jing *et al*., 2014).

2.10.3. Effect of Initial pH of Dye Solution

The solution pH is an important variable in aqueous phase photocatalytic reactions. Since initial pH dictates adsorption and dissociation of organic pollutant, the surface charge properties of the photocatalyst, and size of aggregates formed, oxidation potential of valance band, shifting of valence and conduction band edges, and structure of organic pollutants and other physicochemical properties of the system (Shankar *et al*., 2004). In accordance with Nerst's law, varying the solution pH would shift the energy of the valence and conduction band edges (Hoffmann *et al*., 1995). This results in the conduction band electron becoming more effective and the valence band holes less effective at higher pH.

The pH affects significantly not only photocatalyst activity, but also changes pollutant structure. Low degradation rate at higher pH is attributed to the fact that when the concentration of OH^- ion is higher in the solution, it prevents the penetration of UV light to reach the catalyst surface. Furthermore, high pH favours the formation of carbonate ions which are effective scavengers of OH^- ions and can reduce the degradation rate (Akbal and Onar, 2003; Jing *et al*., 2014).

2.10.4. Effect of Particle Size of the Photocatalyst

Particle size and ultimately, crystallite dimensions play an important role in the photo activity of the semiconductor, since the electron/hole recombination process was showed to be particle size dependent. It is known that in nano meter-size range, the physical and chemical properties

of the semiconductors are modified, when compared to bulk size dimensions. Small variations in particle size leads to great modifications in surface/bulk ratio, thus modifying the significance of volume and surface electron/hole recombination processes. With a smaller particle size (in a nano meter range), the number of active surface sites increases, and so does the surface charge carrier transfer rate in photocatalysis. Some studies revealed that the photocatalytic efficiency does not monotonically increase with decreasing particle size, and there exists an optimal particle size of a few nano meters (3−10 nm) for pure nano crystalline TiO_2 photocatalyst (Zhang *et al.,* 1998).

2.10.5. Effect of Electron Acceptors

In heterogeneous photocatalytic reaction, molecular oxygen (air) has been used for this purpose as an electron acceptor for prevention of electron hole recombination. One approach used to prevent electron hole recombination is to add electron acceptors into the reaction media. The presence of H_2O_2 as electron acceptor can serve as electron scavengers to prevent the recombination and enhance photodegradation efficiency. H_2O_2 has several effects including: (a) avoid recombination of electron-hole by accepting the conduction band electron and (b) increase the concentrations of the hydroxyl radical. Electron scavenging and the consequent e^--h^+ recombination suppression can also be achieved by the use of other inorganic oxidants such as $KBrO_3$ and $(NH_4)_2\ S_2O_8$ (Du *et al.*, 2011).

2.10.6. Effect of Co-existing Ions

Organic dye wastewater composition can vary with time, the basic understanding of the effect of organic and inorganic constituents present in wastewater on the performance of photocatalytic system is crucial to ensure operational stability of a proto type photocatalytic water purification process. A number of studies demonstrated that water components like calcium, magnesium, iron, zinc, copper, carbonate, phosphate, nitrate, sulphate, chloride, and dissolved organic matters can affect the photocatalytic degradation rate of organic pollutants since they can be adsorbed onto the surface of photocatalyt (Abdullah *et al*., 1990; Parent *et al*., 1996). Depending on the solution pH, they can also compete with the target pollutant for the active sites. The adsorption of water components can reduce the formation of OH radicals. Although hydroxyl radical scavenging by the anions bicarbonate, phosphate, nitrate, sulphate,

and chloride resulted in corresponding anion radicals, they have lower oxidation potential. Consequently all these reactions can influence the overall rate of photocatalytic oxidation (Parent *et al*., 1996).

3. MATERIALS AND METHODS

3.1. Experimental Work Site

The synthesis of photocatalysts and photocatalytic degradation experiments were conducted at Haramaya University Chemistry Research Laboratory. The most characterization (XRD, UV-Vis, SEM, BET, and TGA) techniques were conducted at the Institute of Catalysis and Petroleum Chemistry of the CSIC, Madrid, Spain. Moreover, infrared spectroscopy (FTIR) and photoluminescence (PL) studies were then conducted for identification of functional groups and optical intensities of Zr-MOFs at Addis Ababa University.

3.2. Instruments and Apparatus

Different types of materials and chemicals were used during the synthesis, characterization and evaluating photocatalytic degradation experimental works. The materials include; Fourier Transform Infrared Spectrophotometer (Spectrum 65 FT-IR Spectrometer/Perkin Elmer), Fluorlog photoluminescence spectrometer (Horiba Jobin Yvon, Japan), SEM (model

EPMA-8705QH2, Japan), BET (TristarII ,3020), electricity (80W florescent lamp), oven (Gallenkamp, MODEL A050626), centrifuge (Hermle, Z 300, Germany), magnetic stirrer, thermal balance (PERKIN ELMER-TGA 300/15), x-ray diffractometer (XRD, X´Pert Pro PANalytical, PW-3040), UV-Vis spectrophotometer (SANYO, SP65), UV-Vis spectrophotometer (Cary 500 Scan Spectrophotometer) for UV-Vis DRS, analytical balance (Denver Instrument XE-50A), pH-meter (Jenway, MODEL 3320), mechanical shaker (Orbital shaker S01, United Kingdom), photoreactor vessel mortar, micromeritics ceramic crucible, test tubes, deionizer, distiller, pipette, wash bottles, Pyrex glass bottles, filter paper and beakers.

3.3. Chemicals and Reagents

The following analytical grade chemicals were used during the preparation of UiO-66 and UiO-66-NH_2 of Zirconium MOFs in different options. These chemicals are methanol (HPLC, 99.8%, Blulux Ltd-12001), deionized water, $ZrOCl_2$.$8H_2O$ (≥ 99.5%, Aldrich), H_2N-H_2BDC (99%, Aldrich), H_2BDC (98%, Aldrich), H_2O_2 (98%, Blulux LaboratoryLtd-121001), NaOH (98%, BDH, Chemicals Ltd Poole England), TEA (98.5%, Blulux Laboratory Ltd-121001), $NaHCO_3$, $AgNO_3$, DMF (99.8%, Blulux.Pt. No D0206), Sodium chloride (99.5%, Blulux Laboratory Ltd-121001), HCl (Blulux- Laboratory Ltd-121001), Methyl orange (Fisher Scientific Company Cat.No.M-216).

Moreover, the photocatalytic degradation activity of as- synthesized UiO-66 and UiO-66-NH_2 MOFs were studied at HU under visible irradiation, textile waste water sample was collected from the textile factory in Awassa.

3.4. Synthesis of MOFs

UiO-66 and UiO-66-NH_2 MOFs were synthesized in different options by using DIW and DMF as solvents. Room temperature synthesis was done with water as a solvent where as DMF was used in the high temperature synthesis. The as-synthesized MOFs were employed in the subsequent experiment with no further post treatment.

Table 1. Molecular weight (g/mol) of selected chemicals during synthesis of MOF samples

NO	General name	Chemical formula	Molecular weight(g/mol)
1	Zirconium Oxychloride	$ZrOCl_2.8H_2O$	322.25

	octahydrate salt		
2	2-aminobenzene-1,4-dicarboxylic acid	NH_2-BDC	181.15
3	1,4-benzenedicarboxylic acid	H_2BDC	166.13
4	Triethylamine	$(Et)_3N$	101.19
5	Sodium hydroxide	NaOH	39.99

3.4.1. Room Temperature Synthesis of UiO-66-H_2O-RT (Zr)

3.94 g (12.23mmol) of zirconium oxychloride octahydrate salt ($ZrOCl_2.8H_2O$) was dissolved in 50 mL of DIW. 2.03 g (11.21mmol) of benzene dicarboxylic acid (H_2BDC) was dissolved in 50 mL of DIW. 62.85 mmol of NaOH solution (1M) was slowly added into the linker solution drop by drop to deprotonate the organic acid completely. Each mixture was stirred separately for 30 min. Then the metal salt solution was added to the linker solution slowly drop by drop with magnetic stirring and the reaction was equilibrated for 24 h. The precipitate formed was centrifuged at 11000 rpm for 5 min and the product was washed four times with DIW and was filtered. The product was then suspended one times with methanol for three days and then washed three times with methanol overnight and was filtered. Finally the solid was dried in open air at room temperature. The room temperature precipitated Zr-MOF was denoted as UiO-66-H_2O-RT.

3.4.2. Room Temperature Synthesis of UiO-66-NH_2-H_2O -RT (Zr)

1.96 g (6.08mmol) of zirconium oxychloride octahydrate salt ($ZrOCl_2.8H_2O$) was dissolved in 50 mL of DIW. 1.09 g (6.02mmol) of 2-amino-1, 4-benzene dicarboxylic acid (H_2BDC-NH_2) was dissolved in 50 mL of DIW. 25.10 g of NaOH solution (1M) was slowly added in to the linker solution drop by drop to deprotonate the organic acid completely. Each mixture was stirred separately for 30 min. Then the metal salt solution was added to the linker solution slowly drop by drop with magnetic stirring and the reaction was continued for 24 h. The precipitate formed was centrifuged at 11000 rpm for 5 min and the product was washed two times with DIW and the product was suspended with methanol four times overnight and it was centrifuged. Finally, the solid was dried in open air at room temperature. The room temperature precipitated Zr-MOF was denoted as UiO-66-NH_2-H_2O-RT (Zr).

3.4.3. High Temperature Synthesis of UiO-66-DMF-HT (Zr)

3.94 g (12.22 mmol) of zirconium oxychloride octahydrate salt ($ZrOCl_2.8H_2O$) was dissolved in 50 mL of DMF and stirred for 30 min. 2.06 g (12.40 mmol) of benzene dicarboxylic acid (H_2BDC) was dissolved in 50 mL of DMF and stirred for 30 min. Then the metal salt solution was added to the linker solution slowly. Then the sample was placed in an oven set at a temperature of 120^{O}C and reaction was continued for 24 h in the oven. The precipitate formed was centrifuged at 11000 rpm for 5 min and the solid was washed three times with DMF and three times with methanol. Finally the solid was dried overnight in open air at room temperature (Silva *et al*., 2010). The high temperature precipitated Zr-MOF was denoted as UiO-66-DMF-HT (Zr).

3.4.4. High Temperature Synthesis of UiO-66-NH_2-DMF-HT (Zr)

3.94 g (12.22 mmol) of zirconium oxychloride octahydrate salt ($ZrOCl_2.8H_2O$) was dissolved in 50 mL of DMF and was stirred for 30 min. 2.17 g (11.97 mmol) of 2-amino-1,4- benzene dicarboxylic acid (H_2BDC-NH_2) was dissolved in 50 mL of DMF and stirred for 30 min. Then the metal salt solution was added to the linker solution slowly and was stirred for 24 h. The reaction was continued for 24 h in the oven temperature set at 120^{O}C. The precipitate formed was centrifuged at 11000 rpm for 5 min and the solid was washed three times with DMF and three times with methanol. Finally the solid was dried in open air at room temperature and the yield obtained was 5.68 g. The high temperature precipitated Zr-MOF was denoted as UiO-66-NH_2-DMF-HT (Zr) (Shen *et al*., 2014)

3.4.5. High Temperature Synthesis of UiO-66-NH_2-DMF-TEA-HT (Zr)

3.95 g (12.26 mmol) of zirconium oxychloride octahydrate salt ($ZrOCl_2.8H_2O$) was dissolved in 50 mL of DMF and stirred for 30 min. 2.18 g (12.03 mmol) of 2-amino-1, 4-benzene dicarboxylic acid (H_2BDC-NH_2) was dissolved in 50 mL of DMF and stirred for 30 min. Then the metal salt solution was added to the linker solution slowly and stirred for 24 h and then was added 5.02 g (4.96mmol) of TEA to the mixture and stirred for 10 min. The reaction was continued for 24 h in the oven at 120^{O}C. The precipitate formed was centrifuged at 11000 rpm for 5 min and the solid was washed three times with DMF and three times with methanol.

Finally the solid was dried overnight in open air at room temperature. The high temperature precipitated Zr-MOF was denoted as UiO-66-NH_2-DMF-TEA-HT (Zr).

3.4.6. High Temperature Synthesis of UiO-66-DMF-TEA-HT (Zr)

3.95 g (12.26 mmol) of zirconium oxychloride octahydrate salt ($ZrOCl_2.8H_2O$) was dissolved in 50 mL of DMF and stirred for 30 min. 2.08 g (12.52 mmol) of terephatalic acid (H_2BDC) was dissolved in 50 mL of DMF and then 5g (4.96 mmol) of TEA was added to the linker dissolved solution and was stirred for 30 min. Then the metal salt solution was added to the linker solution slowly and was stirred for 24 h. The reaction was continued for 24 h in an oven at 120^{O}C. The precipitate formed was centrifuged at 11000 rpm for 5 min and the solid was washed three times with DMF and three times with methanol. Finally the solid was dried overnight in open air at room temperature. The high temperature precipitated Zr-MOF was denoted as UiO-66-DMF-TEA-HT (Zr).

3.4.7. High Temperature Synthesis of UiO-66-NH_2-H_2O-HT (Zr)

3.906 g (12.12 mmol) of zirconium oxychloride octahydrate salt ($ZrOCl_2.8H_2O$) was dissolved in 50 mL of DIW and stirred for 30 min. 2.02 g (12.16mmol) of 2-amino-1,4- benzene dicarboxylic acid (H_2BDC-NH_2) was dissolved in 50 mL of DIW and stirred for 30 min. Then the metal salt solution was added to the linker solution slowly and stirred for 24 h. The reaction was continued for 24 h in the oven at 120^{o}C. The precipitate formed was centrifuged at 11000 rpm for 5 min and the solid was washed twice with DIW and four times with methanol and then filtered. Finally the solid left was dried in open air at room temperature and weighed. The high temperature precipitated Zr-MOF was denoted as UiO-66-NH_2-H_2O-HT (Zr).

3.4.8. High Temperature Synthesis of UiO-66-H_2O-HT (Zr)

3.906 g (12.12 mmol) of zirconium oxychloride octahydrate salt ($ZrOCl_2.8H_2O$) was dissolved in 50 mL of DIW and stirred for 30 min. 2.02 g (12.16 mmol) of benzene dicarboxylic acid (H_2BDC) was dissolved in 50 mL of DIW and stirred for 30 min. Then the metal salt solution was added to the linker solution slowly and stirred for 24 h. The reaction was continued for 24 h in the oven at 120^{o}C. The precipitate formed was centrifuged at 11000 rpm for 5min and the solid was washed twice with DIW and four times with methanol and then filtered. Finally, the

product left was dried in open air at room temperature. The HT precipitated Zr-MOF was denoted as UiO-66-H_2O-HT (Zr). Finally, the as-synthesized MOFs samples were coded as follows:

Table 2. The as-synthesized MOFs samples and their codes

No	Sample of MOFs	Code	No	Sample of MOFs	Code
1.	UiO-66-H_2O-RT	Z_1	5.	UiO-66-NH_2-DMF-TEA-HT	A_3
2.	UiO-66-NH_2-H_2O-RT	A_1	6.	UiO-66- DMF-TEA-HT	Z_3
3.	UiO-66-DMF-HT	Z_2	7.	UiO-66-NH_2-H_2O-HT	A_4
4.	UiO-66-NH_2- DMF-HT	A_2	8.	UiO-66-H_2O-HT	Z_4

Table 3.Stochiometric amounts of MOFs code, metal salt, bridging ligands, solvents, stirring/reaction time, synthesis condition and finally expected chemical formula of each MOF

MOF code	Z_1	A_1	Z_2 & Z_3	A_2 and A_3	A_4	Z_4
metal salt	$ZrOCl_2.8H_2O$	$ZrOCl_2.8H_2O$	$ZrOCl_2.8H_2O$	$ZrOCl_2.8H_2O$	$ZrOCl_2.8H_2O$	$ZrOCl_2.8H_2O$
Solvent	DIW	DIW	DMF	DMF	DIW	DIW
linker acid	H_2BDC	NH_2-BDC	H_2BDC	NH_2-BDC	NH_2-BDC	H_2BDC
String time(hr)	24	24	48	48	48	48
Condition	RT	RT	HT	HT	HT	HT
expected formula	Z_1, Z_2, Z_3, and Z_4			$Zr_6O_4(OH)_4[C_6H_4(CO_2)_2]_{12}$		
	A_1, A_2, A_3, and A_4			$Zr_6O_4(OH)_4[C_6H_4(CO_2)_2]_{12}$-$NH_2$		

3.5. Characterization of UiO-66 and UiO-66-NH_2

The as-synthesized Zr-MOFs samples were characterized to identify functional groups, optical intensity, structure and crystallinity, thermal stability, topology, surface area (pore volumes) and band gap energy by FTIR, PL, XRD, TGA, SEM, BET and UV-Vis, respectively.

3.5.1. FTIR

In this work, IR spectra were collected on Spectrum 65 FT-IR Spectrometer (Perkin Elmer) in the frequency range (4000-400 cm^{-1}). The IR spectra gave an insight into the nature of the functional groups of metal salt, amine substituted and the organic linker (carboxylic groups) molecules forming the framework structure of the MOFs, namely, whether each group is free or bonded within the structure.

3.5.2. PL

Photoluminescence (PL) spectra were done at Addis Ababa University using a Fluorlog photoluminescence spectrometer (Horiba Jobin Yvon, Japan). The spectra were obtained in the range of 360–560 nm using 310 and 330nm laser excitation.

3.5.3. XRD

The powder diffraction patterns of a given structure are used as a finger print for that specific structure. Hence, the synthesized MOF samples were subjected to powder X-ray diffraction (XRD) using X'Pert ProPANalytical equipped with an X-ray source of a Cu-Ka radiation (wavelength of 0.15406 nm) at step scan rate of 0.02 (step time:1s; 2θ range: 5.0–90.4^{o}). Sizes of the ternary oxide particles were calculated by Debye Scherer equation (Klug and Alexander,1974).

3.5.4. TGA

In this work, TGA was used to detect the thermal stability and to analyze the mass changes occurring on the degradation of the Zr-MOFs structure as function of temperature. Thermogravimetric analysis (TGA) was performed on a thermo gravimetric analyzer PerkinElmer TGA7. Samples were heated at a rate of 20 °C $min^{-1}$to a maximum temperature of 900 °C in a flowing atmosphere of oxygen.

3.5.5. SEM

In this study, the surface morphologies and particle size distribution of the synthesized Zr-MOFs samples were characterized by the scanning electron microscope images registered

using HITACHI Tabletop Microscope TM-1000.

3.5.6. BET

BET theory, proposed by Brunauer, Emmett and Teller is an extension of the Langmuir theory as it incorporates the concept of multi molecular layer adsorption. The micropores surface area and volume values were calculated by BET and Langmuir methods, using the software of this program. The BET surface areas of Zr-MOFs were obtained from N_2 adsorption-desorption isotherms at 77 K on Micromeritics ASAP 2420 device. Prior to measurement, the samples were degassed at 373- 423K depending on the stability of MOFs to remove guest water and unreacted reactants molecules.

3.5.7. UV-Vis Diffuse Reflectance

The optical absorption spectra and band gaps of the as-synthesized photocatalysts were determined using UV/Vis spectrophotometer. The solid state absorbance of the photocatalyst was measured by scanning over the wavelength range of 200 - 900 nm. Using this curve the optical band gap is determined based on Tauc's equation as given below:

$$\alpha h\upsilon = A\,(h\nu - Eg)^{n/2}$$

Where A - is a constant, hν - is photon energy, Eg - is the allowed energy gap, α - is absorption coefficient, n = ½ for allowed direct transition and n = 2 for allowed indirect transition.

3.6. Photocatalytic Degradation Studies of Methyl Orange (MO)

The efficiency of the Zr-MOFs and their respective amine-functionalized Zr-MOFs photocatalysts were studied for photocatalytic degradation of methyl orange (MO) under dark and visible light irradiation. The decolorization of methyl orange was carried out using UV-spectrophotometer to study the absorbance potential of the MOFs. Here, 100 mL (10 ppm) aqueous solution of MO adjusted at pH=4 was poured into 250 mL beaker and 0.15g L^{-1} of the as-synthesized Zr-MOF of interest was added. Initially, the solution was kept in dark for 60 min with continuous stirring to ensure the adsorption-desorption equilibrium of MO solution. Then 6 mL of the solution was withdrawn and centrifuged for 10 min at 4000 rpm and its absorbance was measured as initial stage (A_0).Then the suspension was exposed to visible irradiation. In the event of the experiment, air was purged to the solution to facilitate oxygen

adsorption. Visible light source (fluorescent lamp) having 80W was kept at about 11 cm distance from the beaker containing the suspension. Then 6 mL of the suspension was withdrawn at 20 min interval, centrifuged at 4000 rpm for 10 min to remove the catalyst and its absorbance was measured using UV-Visible spectroscopy at time`t``(A_t). The photocatalytic experiment was undertaken for the duration of 180/240 minutes.

The withdrawn suspension was poured back to the reactor after each absorbance measurement to minimize the effect of photocatalyst amount and MO concentration variation on the efficiency of the degradation process. The spectra of the samples were recorded from 200-800 nm that shows the maximum absorbance at 464 nm (λ_{max}) was taken to calculate percentage degradation. Finally, % degradation of methyl orange using each MOF under dark and visible light can be calculated using the equation given below (Hong *et al*., 2009).

$$\% \text{ Degradation} = \frac{A_0 - A_t}{A_0} \times 100$$

Where, A_o is the absorbance of dye at initial stage, A_t is the absorbance of dye at time "t".

3.7. Study of Point of Zero Charge of the MOF Photocatalyst

As used by Jing *et al*. (2014) and Hasan *et al.* (2016), pH_{PZC} of UiO-66-NH_2-TEA (Zr) was determined by taking nine 100 mL conical flasks and 50 mL of 0.01 M of NaCl solution was added into each flask. All the flasks were labelled and their solution was adjusted to pH of 2, 3, 4, 5, 6, 7, 8, 10 and 12 by using 0.01-1M of HCl and NaOH solutions. Then 0.15 g of the UiO-66-NH_2-TEA (Zr-MOF) was added into each flask and all flasks were transferred to mechanical shaker and shaken for 48 h. Then the pH_{Pzc} was obtained by taking the point at which $\Delta pH = 0$ is the point at which the graph of pH_f and pH_i crosses each other. Finally, the pH of each solution was measured and the result was plotted as pH_f vs pH_i and the point at which the graph crosses each other was taken as PZC of the photocatalyst.

3.8. Effects of Operational Parameters under Visible Light

3.8.1. Effect of Photocatalyst Load

The effect of photocatalyst, (UiO-66-NH_2-TEA (Zr)), load was investigated to find the optimum amount of the catalyst at which the degradation efficiency was higher and to minimize

excess use of catalyst. To this effect, catalyst load ranging from 0.05 gL^{-1} to 0.3 gL^{-1} was taken considering 10 ppm of 100 mL MO solution at pH=4. The catalyst load with higher degradation efficiency was selected for the subsequent experiment.

3.8.2. Effect of Initial MO Concentration

The higher degradation efficiency of initial MO dye concentration was selected. The effect of initial dye concentration of MO solution was done by varying the initial MO concentration from 10ppm to 35ppm at constant photocatalyst (UiO-66-NH_2-TEA-HT) load of 0.15 gL^{-1} at pH = 4. The higher degradation efficiency of initial MO dye concentration was selected for the subsequent experiment.

3.8.3. Effect of pH of MO Aqueous Solution

The effect of pH on degradation efficiency of MO dye was determined by adjusting the pH of MO solution at 2, 4, 6, 8, 10 and 12 using 0.01M, 0.1M and 1M of HCl and NaOH solutions keeping other relevant parameters constant.

3.8.4. Effect of Electron Acceptors

To determine the effect of electron acceptors on the photocatalytic efficiency of the modified Zr-MOF, UiO-66-NH_2-TEA (Zr), the experiment was carried out by using 10 ppm of MO, 0.15 gL^{-1} photocatalyst load of UiO-66-NH_2-TEA-HT (Zr) adjusted at pH=4. Then, 0.1M, 0.2M, 0.3M, 0.4M, and 0.5M concentration of H_2O_2 was added, respectively. Finally, the percentage degradation of MO was calculated and H_2O_2 effect was studied (Samar, 2015).

3.8.5. Effect of Co-existing Ions

To examine the effect of co-existing ions on the adsorption and photocatalytic efficiency of amine-functionalized Zr-MOF, the degradation of MO under dark and visible light was studied. During this study, equal concentration of 0.5gL^{-1} of sodium carbonate and sodium chloride was added keeping other parameters constant. Finally, the percentage degradation of MO was calculated to evaluate the influence of interfering ions on photocatalysis (Shetty *et al*., 2016).

3.8.6. Effect of Amine on Photocatalytic Degradation

To study the effect of amine on the photocatalytic efficiency, some of the Zr-MOFs were amine functionalized and their degradation effect is compared with pure Zr-MOFs (UiO-66). In this

work, 0.15gL^{-1} of each photocatalyst (UiO-66-DMF-HT, UiO-66-NH_2-DMF-HT, and UiO-66-NH_2-DMF-TEA-HT) were added in a beaker containing 10ppm of MO adjusted to pH=4. For the experiment carried out on the real sample, 100 mL of textile effluent was poured into 250 mL beaker and the required parameters were kept similar to the MO dye.

3.9. Mechanism of Photodegradation

To investigate the mechanism for the photodegradation of MO by the photocatalyst, the influence of active species such as superoxide radical (•O_{2-}), hole (h^+) and hydroxyl radical (•OH) in the photodegradation process was studied. Different scavengers were employed individually to remove the corresponding active species so that the function of different active species in the photodegradation process based on the change of photocatalytic conversion of MO is understood. The scavengers used in this study were $NaHCO_3$ for h^+, CH_3OH for OH^- and $AgNO_3$ for superoxide radical (Liu *et al*, 2013). In this work, the experiment was carried out by adding equal concentration of 100 mgL^{-1} of $NaHCO_3$, CH_3OH and $AgNO_3$ as scavengers comprising 10 ppm of initial concentration of MO and 0.15gL^{-1} photocatalyst load at pH = 4.

3.10. Recycling of Photocatalysts

Recycling is a very important parameter to assess the practical application of photocatalysts in wastewater treatment. The effect of reusability of photocatalysts was assessed using the following optimum value: 10 ppm MO concentration, pH=4 and 0.15gL^{-1} photocatalyst (UiO-66-NH_2-TEA-HT) load. The reusability of Zr-MOF photocatalyst contributes significantly to lessen the operational cost. For the catalyst recycling tests, the reaction was performed with recovered catalyst under the same conditions as that used in the first run (Lin *et al*., 2015).

3.11. Real Sample Treatment under Visible Light

As used by Muluneh (2016), degradation of textile effluent from Awassa textile industry, was evaluated using the modified effective photocatalyst, UiO-66-NH_2-TEA (Zr), in optimized

conditions under visible light irradiation with little modification. 100 mL of the sample of textile wastewater was placed in 250 mL beaker by adjusting its pH at 4. Then, 0.15gL^{-1} of photocatalyst load and 0.3M H_2O_2 concentration were added into the solution and the suspension was kept in the dark for 60 min with continuous stirring to ensure the adsorption-desorption equilibrium. In this work, 0.3M H_2O_2 was added to the solution to minimize electron hole-recombination and facilitate more photocatalytic degradation as illustrated in figure 16 (4.2.1.4). Finally, the suspension from the wastewater was irradiated with visible light upon continuous stirring and its absorbance was measured using UV-Visible spectrophotometer at 20 min intervals for 240 min. Then the plot of percent degradation versus irradiation time was plotted.

4. RESULTS AND DISCUSSION

4.1. Characterization of Zr-MOFs

4.1.1. XRD Analysis

Figures (5-6) show the XRD patterns of the as-synthesized MOFs: UiO-66-H_2O-RT, UiO-66-NH_2-H_2O-RT, UiO-66-DMF-HT, UiO-66-NH_2-DMF-HT, UiO-66-NH_2-DMF-TEA-HT, UiO-66-DMF-TEA-HT, UiO-66-NH_2-H_2O-HT, and UiO-66-H_2O-HT, respectively. The diffraction peaks of the above photocatalysts appeared at scattering angles (2θ) of 7.5º, 7.7º, 7.4º, 7.2 º, 7.4º, 5.9º, 7.3º and 7.2º, respectively. All

the diffraction patterns appeared to be similar except UiO-66-DMF–HT and UiO-66-NH_2-DMF-HT, the latter two being highly crystalline as evidenced from the distinctive peaks observed other than the most intense peaks described in figures (5-6). This indicates that the XRD pattern of UiO-66-NH_2 is similar with the UiO-66 topology. These peaks resemble an inner $Zr6O_4(OH)_4$ core in which the triangular faces of the Zr_6 octahedron are alternatively capped by μ_3-O and μ_3-OH groups. The obtained XRD patterns were fairly consistent with published data (Muluneh, 2016; Tsegaye, 2017;Vellingiri *et al* ., 2017).

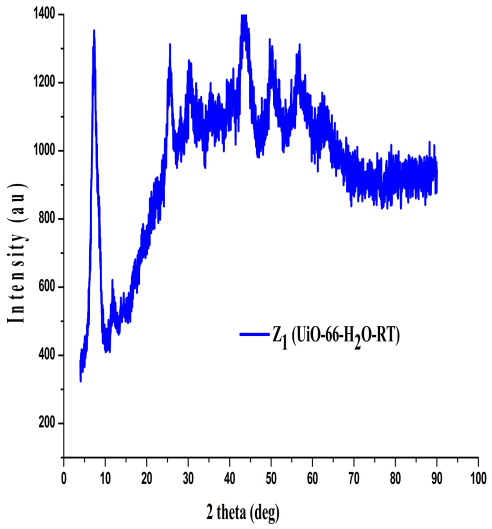

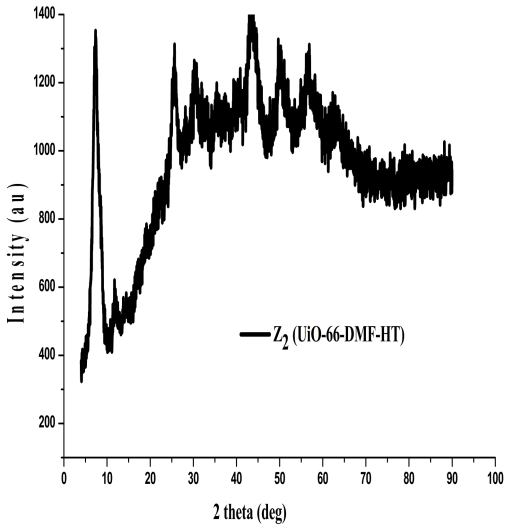

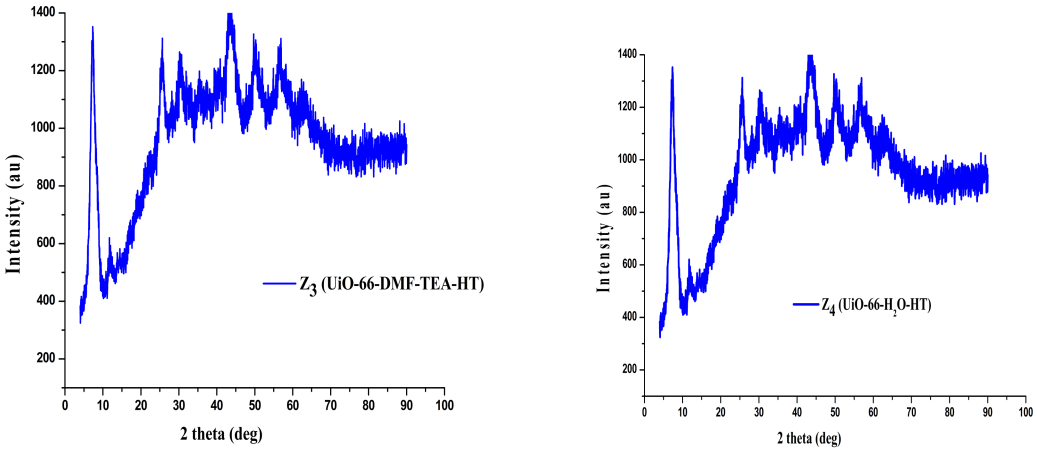

Figure 5. XRD patterns of Zr-MOFs (Z_1, Z_2, Z_3, and Z_4)

Where, Z_1 = UiO-66-H_2O-RT, Z_2 = UiO-66-DMF-HT, Z_3= UiO-66-DMF-TEA-HT, and Z_4 = UiO-66-H_2O-HT

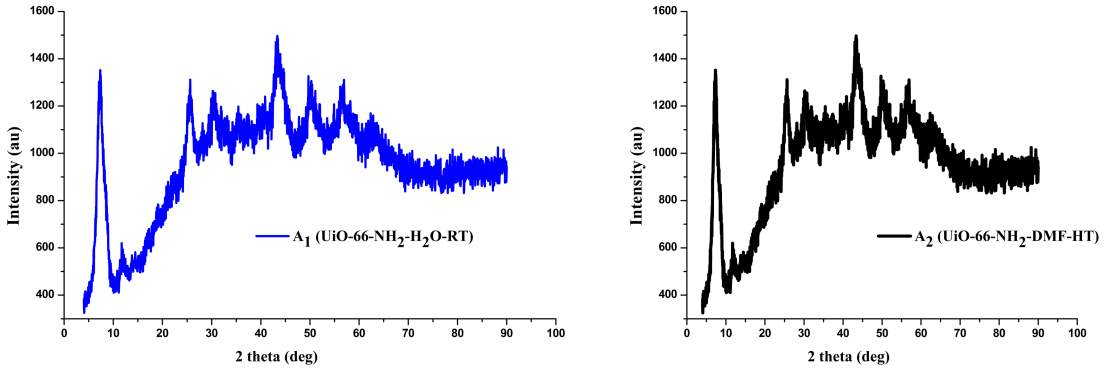

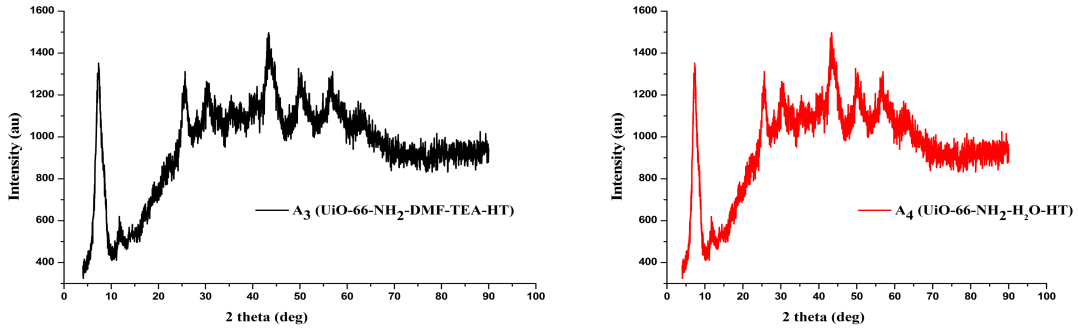

Figure 6. XRD patterns of amine-functionalized Zr-MOFs (A_1, A_2, A_3, and A_4)

Where, A_1 = UiO-66-NH_2-H_2O-RT, A_2 = UiO-66-NH_2-DMF-HT,

A_3 = UiO-66-NH_2-DMF-TEA-HT and A_4 = UiO-66-NH_2-H_2O-HT

The most intense peaks in the XRD patterns were used to calculate the average crystallite sizes (Ds) of as-synthesized of both types of Zr-MOFs. Average crystalline sizes of the as-synthesized Zr-MOFs and modified Zr-MOFs were calculated using Debye-Scherer equation:

$$D = 0.89 \quad / \beta \, Cos$$

Where, β is the full width at half maximum (FWHM), θ is the angle between the incident and diffracted beams in degrees, λ is the X-ray wavelength in nanometres, D is crystallite size.

Table 4. Average crystallite sizes of the as-synthesized Zr-MOFs nanomaterials.

MOF	2θ (degree)	β(radian)	D (nm)	MOF	2θ(degree)	β(radian)	D(nm)
Z_1	7.5	0.0043	32	A_3	7.4	0.0014	98
A_1	7.7	0.0011	118	Z_3	5.9	0.0023	60
Z_2	7.4	0.0074	19	A_4	7.3	0.0031	45
A_2	7.2	0.0061	23	Z_4	7.2	0.0052	27

As shown in Table 4, the average crystallite sizes of as-synthesized photocatalysts were estimated and found in the order: A_1 > A_3 > Z_3 > A_4 > Z_1 > Z_4 > A_2 > Z_2. This is due to the larger BET surface area of Zr-MOFs than respective modified Zr-MOFs. Most of the MOFs, therefore, fall in the nano range.

4.1.2. BET Analysis

BET analyses of Zr-MOFs samples were aimed at to determine the surface areas and the pore volumes of nano particles. As shown Table (5), the increasing BET surface areas of Zr-MOFs are given in the following order: UiO-66-NH_2-H_2O-RT < UiO-66-NH_2-DMF-TEA-HT < UiO-66-DMF-TEA-HT < UiO-66-NH_2-H_2O-HT < UiO-66-H_2O-RT < UiO-66-H_2O-HT < UiO-66-NH_2- DMF-HT < UiO-66-DMF-HT.

Table 5. The BET surface areas and total pore volumes of the as-synthesized Zr-MOFs

Sample Code	BET (m^2/g)	Total Pore volume (cm^3/g)	Sample Code	BET (m^2/g)	Total Pore volume (cm^3/g)
Z_1	303	0.473758	A_3	235	0.242355
A_1	168	0.295350	Z_3	250	0.582034
Z_2	764	0.590434	A_4	282	0.442932
A_2	549	0.371729	Z_4	337	0.454854

In this result one could realize the effect of solvent, temperature and modulators. The effect of solvent is observed when we compare $Z_{2/4}$ Vs $A_{2/4}$. As one can note from Table 5, DMF performed better than water as a solvent in synthesizing MOFs of higher specific surface area. The effect of synthesis temperature on the surface area of MOFs is also revealed from the BET results of $A_{1/4}$ Vs $Z_{1/4}$. Higher surface area is witnessed for MOFs prepared at higher temperature compared to the room temperature approach. Introduction of TEA as modulator resulted to lower BET perhaps due to incorporation of solvents into the pores of the as-synthesized MOFs. Based on the above discussion, one could infer the following generalization; zirconium MOFs showed higher BET surface areas than their corresponding modified zirconium MOFs. Similar reports have been obtained by previous researchers (Chen *et al*., 2015).

4.1.3. Analysis of UV-Vis Diffuse Reflectance Spectroscopy

The UV-Vis Diffuse Reflectance Absorption Spectra of the Zr-MOFs nanomaterials were recorded. Accordingly, band gap energies (E_g) of the as-synthesized nanoparticles were obtained from the Tauc plot. Tauc plot is one method of determining the optical band gap in semiconductors. The square root of the product of the absorption coefficient and photon energy versus photon energy was plotted in the Figure 7. The curve has a section of straight line. Using this curve the optical band gap energy was determined based on Tauc's equation (Cao *et al*., 2012) shown below.

$$\alpha h\nu = A\,(h\nu - Eg)^{n/2}$$

Where α, hν, A, and Eg are optical absorption coefficient, the photonic energy, proportionality constant, and band gap, respectively. In addition, n = ½ for allowed direct transition and n = 2 for allowed indirect transition was used.

In Figure (7), the direct band gap energies of the as-synthesized photocatalysts were determined from the plot of $(\alpha h\nu)^2$ vs. hν. Accordingly, the direct band gap energy estimated by extrapolating the straight line to the x-axis for UiO-66-H_2O-RT, UiO-66-NH_2-H_2O-RT , UiO-66-DMF-HT, UiO-66-NH_2-DMF-HT, UiO-66-NH_2-DMF-TEA-HT, UiO-66-DMF-TEA-HT ,UiO-66-NH_2-H_2O-HT and UiO-66-H_2O-HT were found to be 3.47 eV, 2.59 eV, 3.86 eV, 2.74 eV, 2.23 eV, 3.44 eV, 3.21 eV and 3.52 eV, respectively. Among the above list, the band gap energy of UiO-66-NH_2-DMF-TEA-HT was the least (2.23 eV) and exhibiting the red-shift making it amenable for visible light irradiation based photocatalysis.

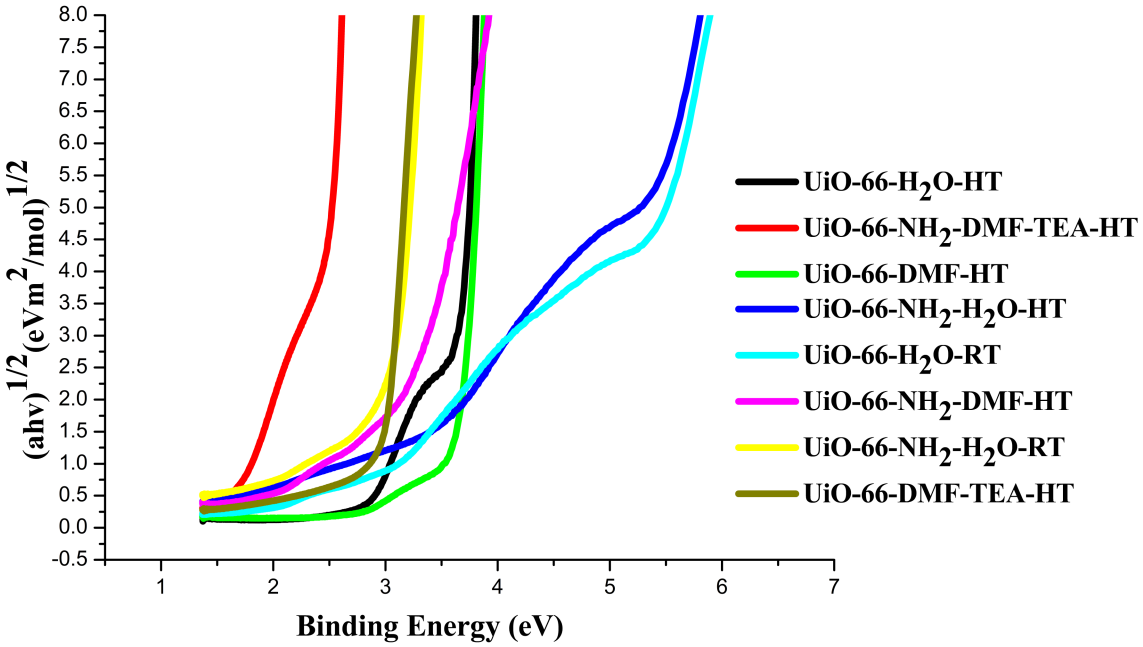

Figure7. Kubelka-Munk-transformed diffuse reflectance spectra of Zr- MOFs and their respective modified Zr-MOFs.

4.1.4. Photoluminescence (PL) Study of As-Synthesized Photocatalyst

The PL studies of as-synthesized Zr-MOFs were used to investigate the life time of the photogenerated electrons and holes and in turn to determine electron-hole recombination properties. The photoluminescence spectra of Zirconium MOFs are shown in Figure 8. It was observed that PL intensity of amine-functionalized Zr-MOF is much lower as compared to respective Zr-MOF. In amine-functionalized Zr-MOF, photo induced charge carrier generation of electrons and holes can be effectively separated and consequently the PL intensity goes down (Long *et al*., 2012). This is because; lower the excitonic PL intensity, stronger the

competence of amine functionalized MOF to confine photo-induced electrons. The higher the separation rate of photo induced electrons and holes, the higher the photocatalytic activity. The order of intensity is UiO-66-DMF-HT > UiO-66-H_2O-RT > UiO-66-DMF-TEA-HT > UiO-66-NH_2-DMF-HT > UiO-66-NH_2-H_2O-RT > UiO-66-NH_2-DMF-TEA-HT. This trend is in good agreement with the results obtained for photocatalytic degradation curves presented in Figure 12. From the above order one can infer that the amine functionalized Zr-MOF (UiO-66-NH_2-DMF-TEA-HT) showed relatively higher efficiency for photocatalytic degradation of MO. Hence, the modification of Zr-MOF with amine (NH_2-BDC) gave evidence for enhancing the photocatalytic activity of the as-synth esized Zr-MOF. Similar result is observed by Musho *et al*., (2014).

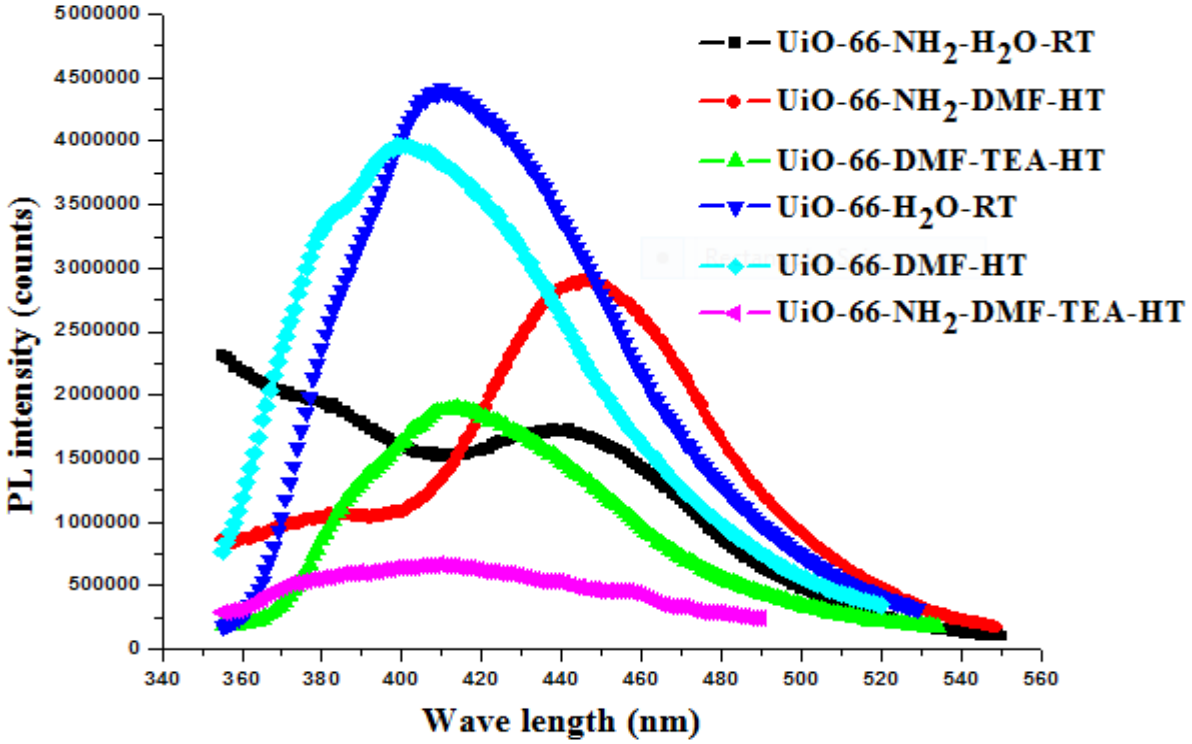

Figure 8. Photoluminescence spectra of as-synthesized Zr-MOFs and their modified Zr-MOFs

4.1.5. SEM Analysis

The surface morphological features of selected Zr-MOFs were observed by using the SEM images. The naked nano-composites corresponding SEM images are shown subsequently in Figure 9 (a, b, c, d). The SEM micrographs in all cases show irregular shaped particles with no distinct morphology. The figures correspond to the SEM images of as-synthesized Zr-MOFs, UiO-66-DMF-HT, UiO-66-H_2O-RT, UiO-66-NH_2-H_2O-RT and UiO-66-NH_2-DMF-HT, respectively. Almost all selected Zirconium MOFs are composed of

irregularly shaped particles due to the intergrowth of the MOF crystals and non homogeneous particle size distribution was observed. But UiO-66-NH_2-DMF-HT has good homogeneous particle size distribution and relatively definite crystal shape has been observed.

Generally, the SEM images indicated that the powders of all the as-synthesized Zr-MOFs were composed of mostly irregular shaped crystal particles. Moreover, the result of UiO-66-NH_2-DMF-HT related to literature report (Lin *et al*., 2015). Some Zr-MOFs in this study are different from those in the literature in which the MOFs were synthesized by methods providing better crystal formation (Silva *et al*., 2010).

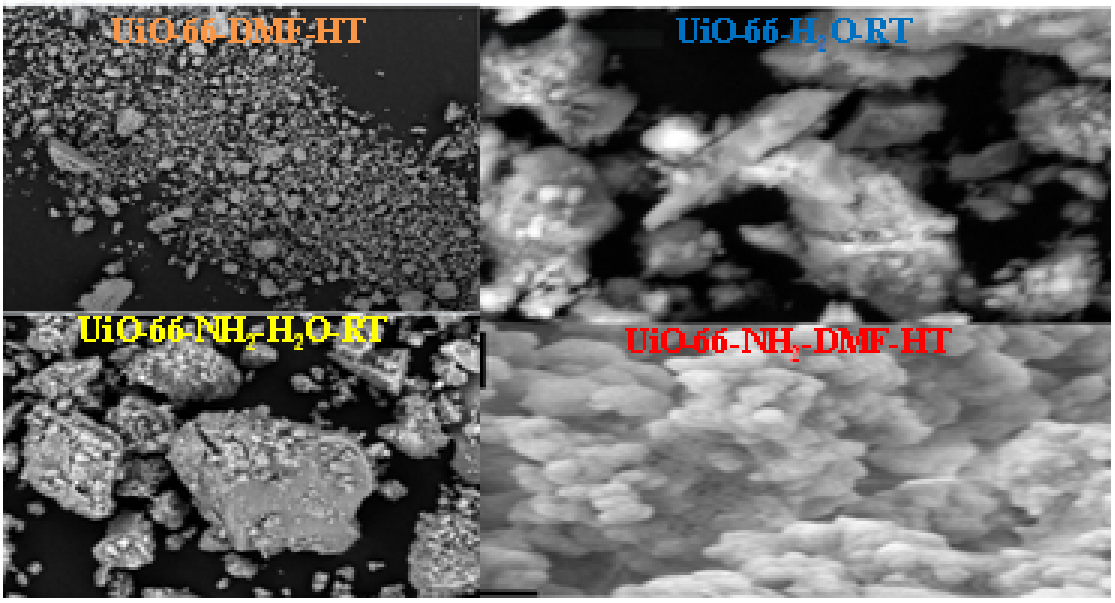

Figure 9. SEM images of UiO-66-DMF-HT, UiO-66-H_2O-RT, UiO-66-NH_2-H_2O-RT and UiO-66-NH_2-DMF-HT, respectively.

4.1.6. FTIR Analysis

Two of the Zr-MOFs with high adsorption and photocatalytic efficiency were selected as representatives to investigate the typical functional groups. Accordingly the FTIR of

UiO-66-DMF-HT and UiO-66-NH_2-DMF-TEA-HT was conducted in the range from 4000 to 400 cm^{-1} (Figure 10).

UiO-66-NH_2–DMF-TEA-HT displays two absorption bands when compared with the IR spectrum of UiO-66-DMF-HT (Shen *et al*., 2014). This is due to the aromatic amino groups which display two medium absorptions, one at 3456 cm^{-1} and the other at 3349 cm^{-1}. These bands represent, respectively, the asymmetric and symmetric N-H stretching modes. At the lower frequency range, bands at 1438 cm^{-1} and 1258 cm^{-1} represent the C-N stretching modes. The band at 1660 cm^{-1} could be attributed to N-H bending frequency (Lin *et al*., 2012; Lin *et al*., 2016). The band at 1580 cm^{-1} could be attributed to C-O bonding in the carboxylate (Lin *et al*., 2016) and the band at 1438 cm^{-1} was from the C-C vibration mode (Lin *et al*., 2015). The band at 782 cm^{-1} was attributed to N-H rocking vibration bonding in the amine group (Lin *et al*., 2016). In both MOFs, the band at 1372 cm^{-1} can be attributed to the C=O bonding in the carboxylate and residue probably due to atmospheric CO_2 (Chira *et al*., 2011).

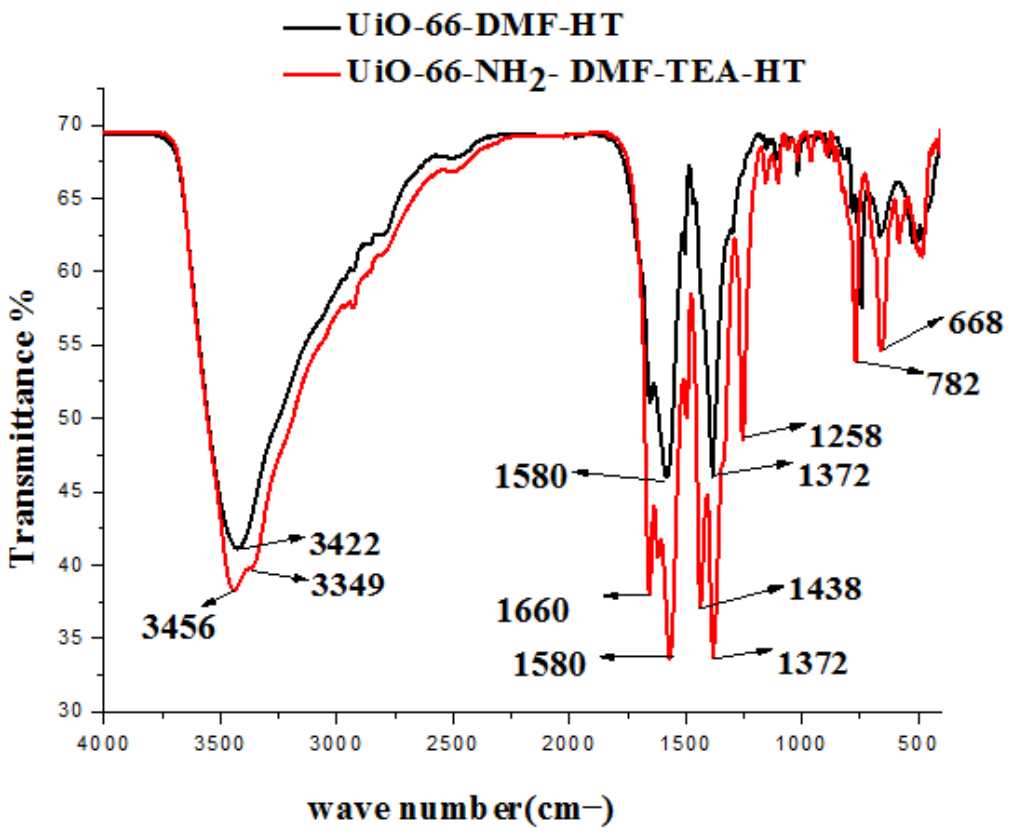

Figure 10. FTIR spectra of various selected Zr-MOFs.

4.1.7. TGA Analysis

As shown in Figure 11, the TGA profile shows 27% weight loss pattern for the MOF, UiO-66-DMF, in the temperature range of 50 - 130 ^{o}C. This may be due to the removal of surface adsorbed DMF and methanol molecules used for the synthesis. Additional sharp weight loss (44%) was also observed around 600 ^{o}C, which may be attributed to the structural

collapse of the MOF into its oxide as the result of decomposition of the organic linker molecules. The thermo gram of UiO-66-H_2O shows a significantly low weight loss (5%) in the range of 50 - 80 ^oC. This may be attributed to the removal of surface adsorbed moisture (water) and methanol molecules. In addition, 35% weight loss was observed around 543 ^oC, which may be indicative of the decomposition of the MOF into its oxide. The residual weights after heating the samples, UiO-66-DMF and UiO-66-H_2O, at 950 ^oC were 29% and 60%, respectively. Thus, we can conclude that room temperature synthesized Zr-MOF has more oxide content than the high temperature synthesized one. Besides the Zr-oxide (cluster) residual weight (%) obtained for UiO-66-DMF was in a good agreement with the theoretical value reported (25.7%) previously by Muluneh (2015). Such a temperature range reveals the high thermal stability of UiO-66(Zr-MOF).

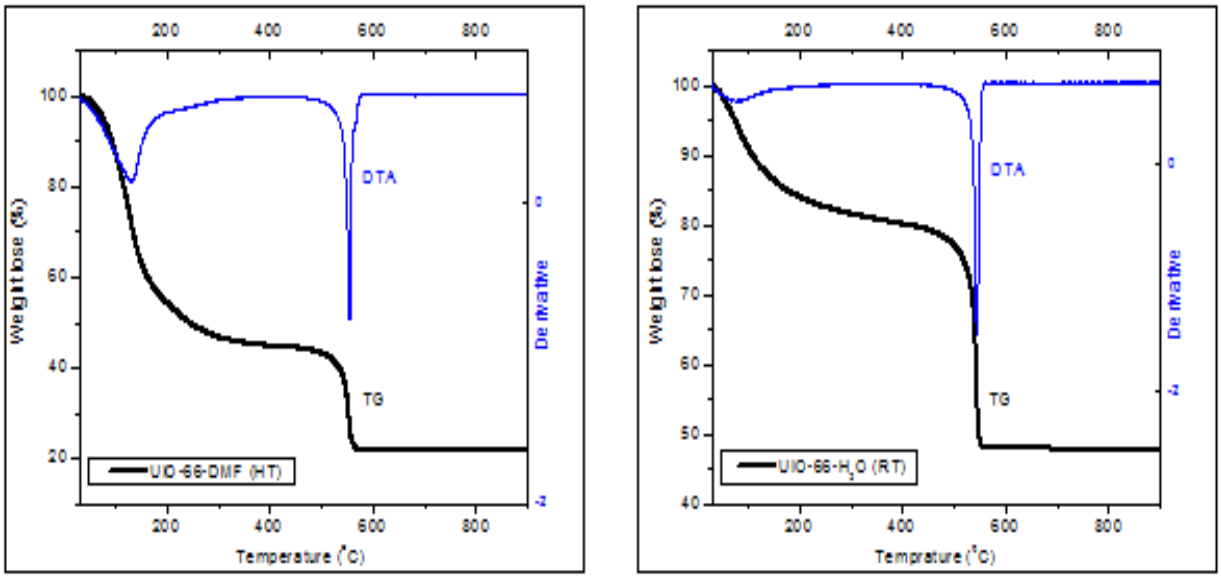

Figure 11. Thermo gravimetric analysis (TGA) of Zr-MOFs

4.2. Photocatalytic Degradation of MO under Visible Light Irradiation

The dark adsorption and percent degradation (initiated by visible light irradiation) of MO by employing different Zr-MOFs were studied using 10 ppm of initial MO concentration with

0.15g L^{-1} of catalyst load. The percentages of model pollutant (MO) removed versus irradiation time of different Zr-MOFs and their modified Zr-MOFs were plotted in Figure 12. Figure 12 and appendix Table 1 clearly indicated that the degradation efficiency of: UiO-66-DMF-HT < UiO-66-H_2O-HT < UiO-66-H_2O-RT < UiO-66-DMF-TEA-HT < UiO-66-NH_2-H_2O-HT < UiO-66-NH_2-DMF-HT < UiO-66-NH_2-H_2O-RT < UiO-66-NH_2-DMF-TEA-HT. Their corresponding degradation percentages are; 19.86%, 28.03%, 40.02%, 43.32%, 47.23%, 49.03%, 54.38%, and 58.92%, respectively. UiO-66-NH_2-DMF-TEA-HT is found to exhibits the highest photocatalytic activity due to reduced band gap (2.23 eV) making it sensitive to visible irradiation and low electron-hole recombination center as evidenced in the PL spectra of this material (Figure 8).

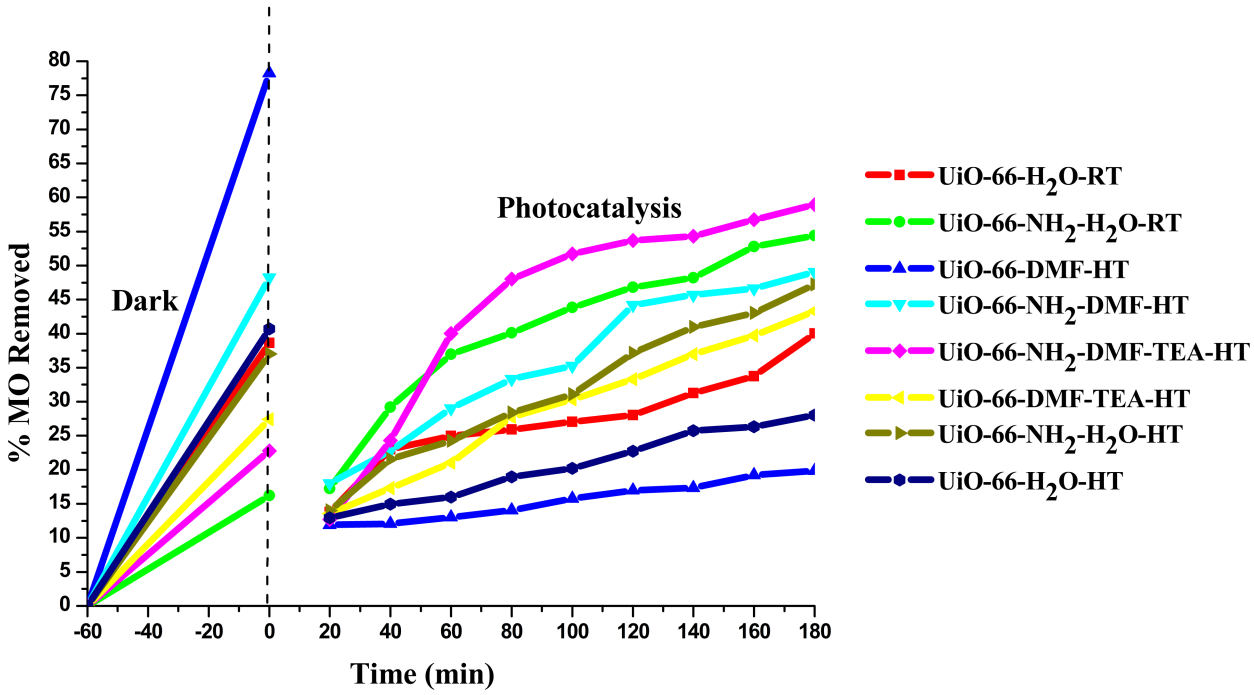

Figure 12. Degradation of MO using Zr-MOFs photocatalysts under visible light illumination (Initial MO = 10 ppm, Photocatalyst load = 0.15gL^{-1}).

Generally, the degradation efficiency of UiO-66-NH_2-DMF-TEA-HT (Zr) was found to be more than the other Zr-MOFs which may be due to its lower optical intensity under PL study and its lower band gap energy (2.23eV) that broaden the absorption wavelength to the red portion of the visible spectrum.

On the other hand, the adsorption efficiency followed the order: UiO-66-DMF-HT > UiO-66-NH_2-DMF-HT > UiO-66-H_2O-HT > UiO-66-H_2O-RT > UiO-66-NH_2-H_2O-HT >

UiO-66-DMF-TEA-HT > UiO-66-NH_2-DMF-TEA-HT > UiO-66-NH_2-H_2O-RT. The adsorption percentages are: 78.24%, 48.24%, 40.71%, 37.02%, 27.38%, 24.41%, 22.78%, and 16.21%, respectively .The highest adsorption efficiency of UiO-66-DMF-HT was observed in the dark due to its largest BET surface area (763.9m^2/g) and the highest pore volume (0.59 cm^3/g). Among Zr-MOFs of this work, UiO-66-DMF-HT was the best sorbent and can remove more MO from aqueous solution by sorption than by photocatalysis which is line with Muluneh (2016).

In general, one could extract the following generalization from the above discussion. The MOFs performed best in the dark are performed less in the visible irradiation and vice versa. However, from the point of view of getting the best material for the removal of the dye, both mechanisms (sorption and photocatalysis) can work in synergy to fabricate what is called a hybrid photocatalyst. In studying the effect of operating parameters for photocatalytic degradation of MO by MOFs, UiO-66-NH_2-DMF-TEA-HT was selected for photocatalytic parameters experiment.

4.2.1. Effect of Operational Parameters on MO Degradation under Visible Light

4.2.1.1. Effect of pH

The adsorption as well as the photocatalytic degradation of model pollutant (MO) and organic dye-containing wastewater reactions is influenced not only by the initial dye concentration but also by initial pH the solution. Hence, to study the effect of pH on degradation of MO dye solution, the pH was adjusted from 2.0 to 12.0 keeping initial dye concentration at 10 ppm and photocatalyst load of 0.15gL^{-1}.The percentage of MO removed verses contact time was plotted as shown in appendix Table 2 and Figure 13.

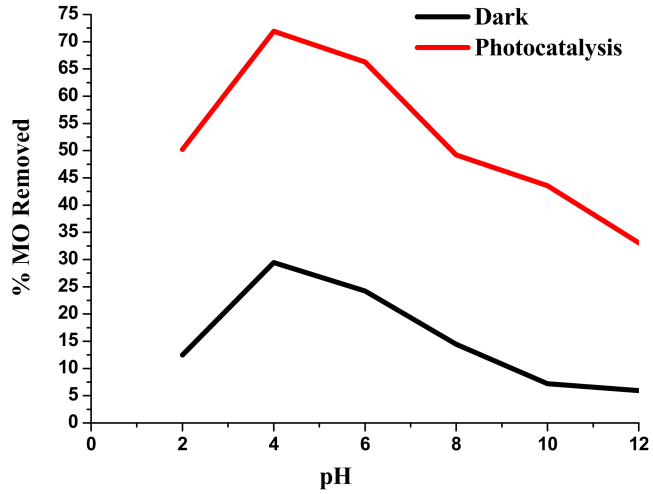

Figure 13. Effect of initial pH on the degradation of MO under dark and visible light illumination

In appendix Table 2 and Figure 13, the experimental results revealed that the as-synthesized amine-functionalized Zr-MOF (UiO-66-NH_2-DMF-TEA (Zr)) could work effectively for both adsorption and degradation of MO at a pH range of 2.0 to 4.0 and this indicates the percentage of degradation is higher at acidic condition than the basic condition. Because MO is an anionic dye, its structure becomes negatively charged when it is dissolved in water. As the pH is reduced, the functional groups are protonated, thus raising the positive charge of photo catalyst surface.

The surface of photocatalyst will be charged positively at lower pH and results in the increased adsorption of anionic molecules while in the reverse situation it would adsorb cationic molecules very easily (Mittal *et al*., 2007). The higher adsorption and degradation of MO may result from electrostatic attraction between the positively charged photocatalyst (UiO-66-NH_2-DMF-TEA (Zr)) ($pH_{Pzc} < 6.04$) surface and the negatively charged anionic MO dye.

However, the photocatalytic degradation of MO gradually decreased at higher pH of MO which may be due to the presence of repulsion between at higher concentration of OH^- ions of

photocatalyst surface (pH_{pZC} > 6.04) and an anionic dye of MO in turn the condition prevent the penetration of Visible light (Shetty *et al*., 2016).

In addition, at higher pH there is also a high probability of carbonate ions formations which are effective scavengers of OH^- ions that can reduce degradation rate (Shankar *et al*., 2004; Jing *et al*., 2014). The highest photocatalytic degradation efficiency (79%) was obtained at pH 4 after 180 min. The general trend is, however, similar to previous studies done for photocatalytic degradation of MO dyes with iron MOFs (Muluneh Endashaw, 2016).

4.2.1.2. Effect of photocatalyst load

The quantity of photocatalyst during photodegradation of MO under visible irradiation is one of the core parameters for the degradation of substrate to application and cost of photocatalyst. In order to avoid the use of excess photocatalyst, it is essential to find out optimum load of the photocatalyst for efficient removal of dye. Hence, a serious of experiments was carried out to find the optimum amount of the photocatalyst (UiO-66-NH_2-TEA-HT (Zr)) load. Accordingly, photocatalyst load ranging from 0.05 gL^{-1} - 0.3gL^{-1} was employed keeping the initial dye concentrartion at 10 ppm with a pH adjusted 4. The percent adsorption and degradation of organic dye versus irradiation time by varying the photocatalyst amount was recorded in appendix Table 3 and plotted in Figure 14 below.

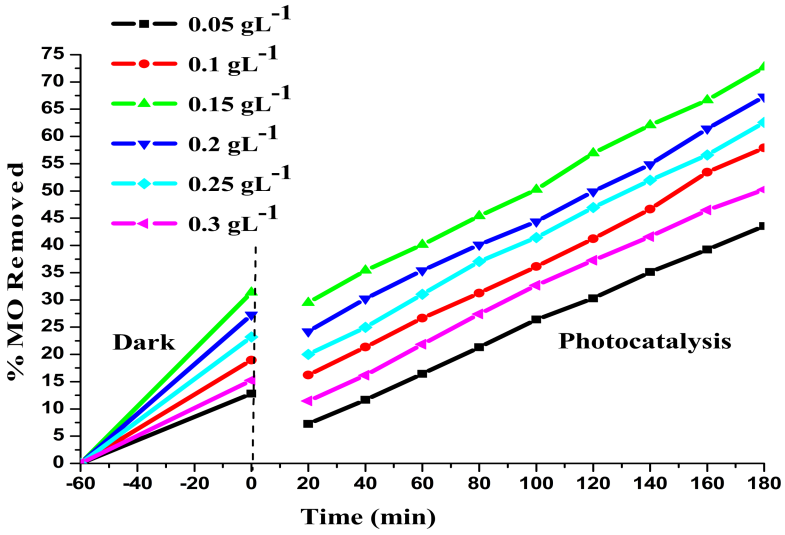

Figure 14. Effect of photocatalyst load on the degradation of MO using modified Zr-MOF photocatalysts under dark and visible light illumination (Initial dye concentration=10ppm with pH adjustment at 4).

As shown in appendix Table 3 and Figure 14, the dark adsorption results of photocatalyst load for 0.05 gL^{-1}, 0.1 gL^{-1}, 0.15 gL^{-1}, 0.2 gL^{-1}, 0.25 gL^{-1} and 0.3 gL^{-1} were 13%, 19%, 31%, 27%, 23% and 15% respectively. Moreover, the percent degradation results for those consecutive photocatalyst load were 44%, 58%, 72%, 67%, 64% and 50% respectively. As a result, the overall dark adsorption and degradation results revealed that the rate of adsorption plus degradation increases when the photocatalyst load was increased from 0.05 - 0.15 gL^{-1} in which the adsorption was from 13% to 31% and the degradation was from 44% to 73%.

However, both sorption and degradation efficiency was decreased when the amount of the photocatalyst was further increased from 0.2 - 0.3 gL^{-1}. It is evidently observed from Figure (14) that the initial degradation rate increases proportionally with the amount of the

photocatalyst only up to some fixed point due to the increase in the total active sites available for the photocatalytic reaction as the dosage of photocatalyst increased but further progressive increase in the amount of the photocatalyst decrease the degradation efficiency may be due to the aggregation of catalyst particles at high concentrations, causing a decrease in the number of surface active sites and the level of light penetration in the reaction medium. Here, the visible light penetration was decreased as result of shielding effect of the overdosed suspended particles of the photocatalyst. When the concentration of the solid particles is higher, the tendency of particle-particle interaction (agglomeration) increases that reduces the surface area available for light absorption and decreases photocatalytic degradation rate (Sobczynski *et al*., 2004).

4.2.1.3. Effect of initial MO concentration

Initial dye concentration is one of the main parameters to study the efficiency of photocatalysts during photocatalytic degradation of any organic dye-containing wastewater. The experimental results were conducted to study the effect of initial MO aqueous solution by plotting percent degradation of MO as a function of irradiation time at varying dye initial concentration (10ppm to 35ppm) using a fixed amount of 0.15 gL^{-1} photocatalyst (UiO-66-NH_2-TEA(Zr) load as shown in Figure 15 and appendix Table 4.

As shown in appendix Table 4 and Figure 15, the result clearly accounted that as the initial dye concentration increases both the adsorption and photocatalytic degradation of MO decreases. The adsorption results of initial dye concentration for 10 ppm, 15 ppm, 20 ppm, 25 ppm, 30 ppm and 35 ppm were 37%, 27%, 23%, 19%, 15% and 12% ,respectively.

Moreover, the photocatalytic degradation results for those consecutive initial dye concentrations were 72%, 64%, 57%, 52%, 46% and 39%, respectively. In general, the overall percentage of sorption-photocatalysis decreased when the initial MO concentration was increased from 10 ppm to 35 ppm. This may be due to a fixed active cites of photocatalyst the role which can be suppressed by the oversaturation of the dye molecules which in turn causes prevention of the visible light penetration from reaching the surface of the photocatalyst. This effect resulted in the reduction of the photogeneration of relative amount of $^{\bullet}OH$ and $^{\bullet}O_2^-$ on

the surface of the catalyst with the intensity of light and irradiation time and hence degradation rate decreases (Zhu *et al*., 2000; Jing *et al*., 2014).

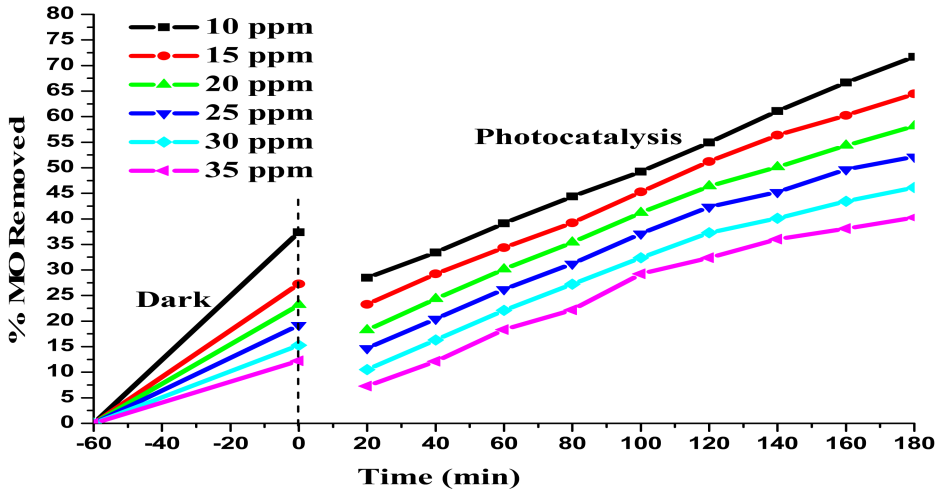

Figure 15. Effect of initial dye concentration on the degradation of MO using modified Zr- MOF photocatalysts under dark and visible light illumination (photocatalyst load=0.15 gL^{-1} and with pH adjustment at 4).

4.2.1.4. Effect of electron acceptors

Electron acceptors such as H_2O_2 are believed to improve the photocatalytic degradation of organic dye pollutants by preventing electron-hole recombination by accepting the CB electron and by generating more OH• radicals and other oxidizing species, as illustrated in the equations (4.1-4.4) (Samar, 2015).

$$H_2O_2 + h\nu \rightarrow 2OH\bullet \quad (4.1)$$

$$H_2O_2 + O_2\bullet^- \rightarrow OH\bullet + OH^- + O_2 \quad (4.2)$$

$H_2O_2 + e^-_{CB} \rightarrow OH\bullet + OH^-$ (4.3)

$H_2O_2 + OH\bullet \rightarrow H_2O + HO_2\bullet$ (4.4)

OH• radical plays significant role in the photocatalytic degradation of organic dye after the addition of hydrogen peroxide (H_2O_2). As shown in Figure (16), the photocatalytic degradation of MO was studied by using effective amine-functionalized Zr-MOFs under dark and visible radiation upon addition of different concentrations of H_2O_2 (0.0M-0.5M) using other parameters kept constant.

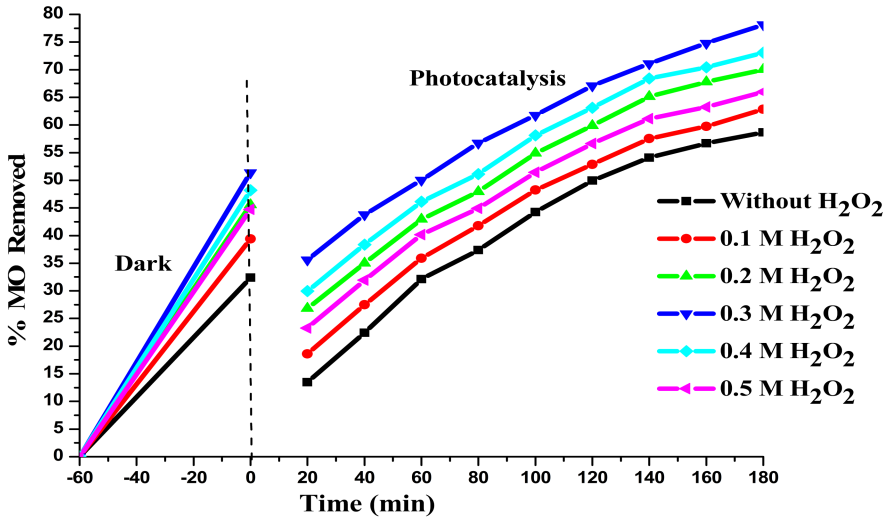

Figure 16.Effect of H_2O_2 on the degradation of MO using modified photocatalysts under dark and visible light illumination (photocatalyst load = 0.15gL^{-1}, 10ppm of MO, 0.0M- 0.5M of H_2O_2 at pH=4 adjustment).

As shown in Figure 16 and appendix Table 5, the adsorption plus the photocatalytic degradation of MO was the least upon addition of 0.1M of H_2O_2, but the highest up on the addition of 0.3M of H_2O_2. The effect of H_2O_2 concentration on enhancing photocatalytic

degradation of MO is given in the following order: 0.3 M > 0.4 M > 0.2 M > 0.5 M > 0.1 M > 0.0 M

The result revealed that both sorption and visible degradation of MO increased with increasing H_2O_2 concentration up to 0.3 M due to increased OH• that are responsible for enhancing photooxidation of the dye molecules (better mineralization rate). However, increasing the concentration of the scavenger concentration beyond the optimum have showed a reverse effect due to H_2O_2 that might act as a scavenger of valence band holes and OH• which is the main oxidative species, when present at too high concentrations, forming HO_2• which is less reactive than OH• (Samar, 2015; Konstantinou, 2004).

4.2.1.5. Mechanism of Photocatalytic Degradation

The photocatalytic mechanism of the modified Zr-MOF was investigated through determining the potential roles of HO•, O_2^{-}•, and h^+ during the degradation of MO, since they are known as the three main active species involved in the photocatalytic oxidation process (Hoffmann *et al*., 1995; Hernandez-Alonso *et al*., 2009). To spot the contributions of these active species, three different scavengers, CH_3OH, $AgNO_3$, and $NaHCO_3$ were separately introduced in the degradation process to attempt to trap HO•, O_2^{-}•, and h^+. Accordingly, 10 ppm of MO and 150 mgL^{-1} of UiO-66-NH_2-TEA-HT adjusted at pH 4 was used to carry out the degradation experiment.

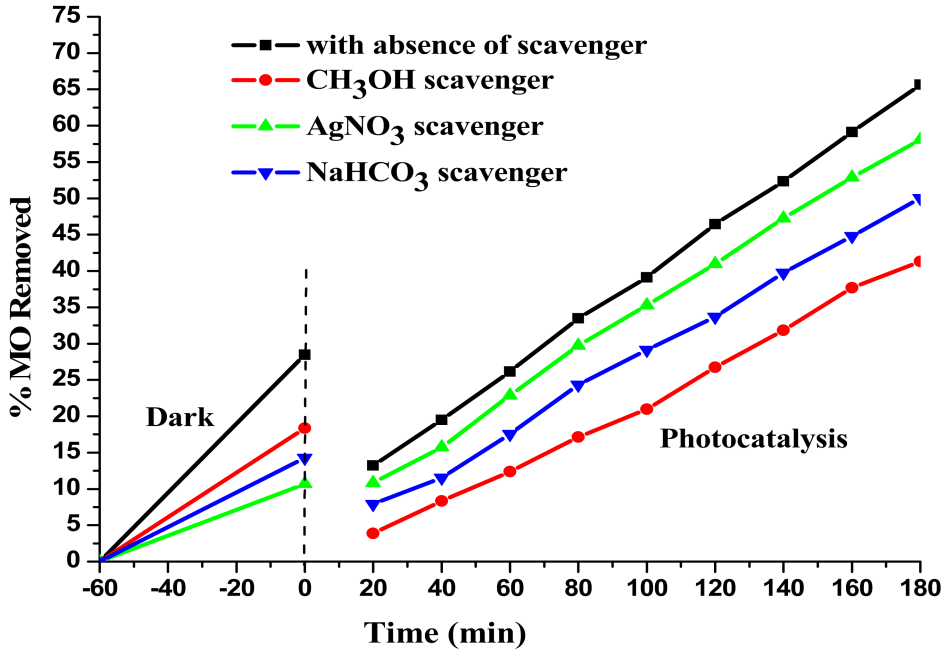

Figure 17. Mechanism of Photocatalytic Degradation in the presence of modified photocatalysts under dark and visible light illumination

The result showed that the percentage adsorption of MO under dark in the absence/presence of scavengers such as $NaHCO_3$, CH_3OH and $AgNO_3$ were found to be 8.46%, 18.38%, 10.68%, and 14.28%, respectively. The percentage of MO removed under visible light in the absence /presence of scavenger such as CH_3OH, $AgNO_3$, and $NaHCO_3$ were found to be 66%, 56%, 47% and 41%, respectively. Addition of CH_3OH enhances degradation of MO relative to other scavengers. We observed in this experiment that the least and the highest percentage degradation of MO were obtained when $NaHCO_3$ and CH_3OH were added as scavengers.

$NaHCO_3$ is able to suppress the generation of h^+ in the valence band, which may not only suppress the activity of h^+, but also accelerate the recombination of e^- and h^+. Thus, the formation of O_2-• was also suppressed in the presence of $NaHCO_3$. Hence, the degradation of MO was almost restrained by $NaHCO_3$ due to the limited generation of h^+ and O_2-•. On the other hand, $AgNO_3$ is O_2-• quencher, O_2-• should be the other main active species participating in the decomposition process of MO. However, the addition of CH_3OH showed relatively less pronounced degradation compared to $NaHCO_3$ and $AgNO_3$. Consequently, O_2-• and h^+ are the main active species in the photodegradation of MO.

4.2.1.6. Effect of Co-existing Ions

The presence of co-existing ions in different amounts in industrial waste water affects the photocatalytic degradation of pollutant (Bhatkhande *et al*., 2001; Pujara *et al.,* 2007). Due to this fact, the effect of co-existing anions on both sorption and photocatalytic degradation of MO was examined using equal concentrations ($0.5gL^{-1}$) of salts at initial dye concentration of 10ppm and catalyst load of $0.15gL^{-1}$ the results of which is depicted in Figure 18.

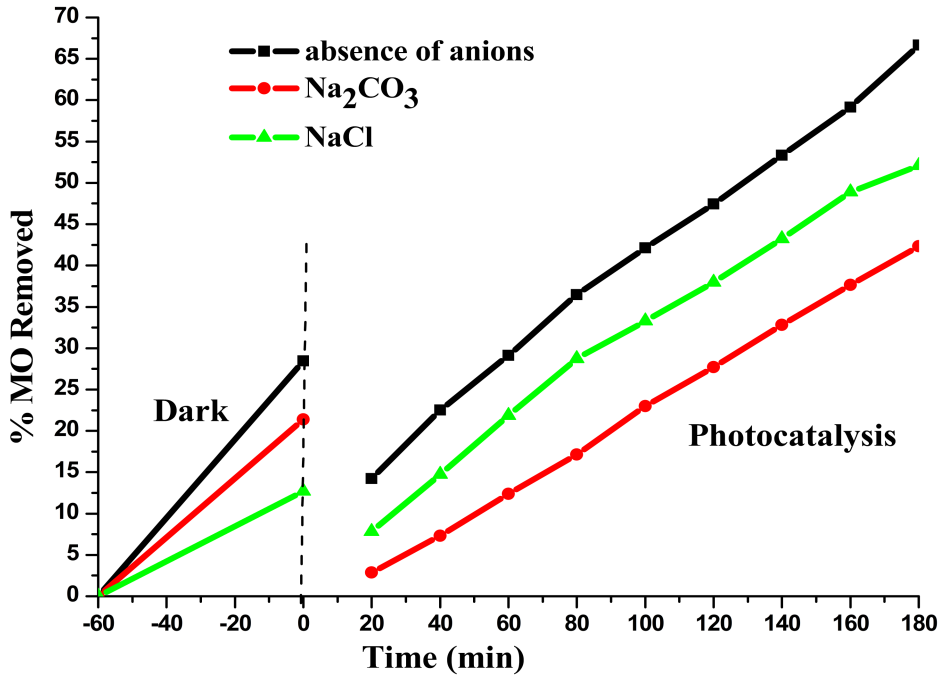

Figure 18. Effect of co-existing anions on the degradation of MO using modified Zr-MOFs under dark and visible light illumination

Results from the above graph evidenced the significant effect of co-occurring anions such as Cl^-, CO_3^{-2} in suppressing photodegradation. These ions could be radical scavengers and react with OH• radicals, which were supposed to attack the dye molecules and convert the same to simpler fragments or molecules. Previous study concluded that carbonate anions have negative effect on photocatalytic degradation (Kamble *et al*., 2006).

$Cl^- + hvb^+ \rightarrow Cl\bullet$

(4.5)

$CO_3^{-2} + OH\bullet \rightarrow OH^- + CO_3\bullet^-$

(4.6)

Both anions were found to inhibit photocatalysis, with the order of $Cl^- > CO_3^{-2}$. The decline in photocatalytic degradation of MO clearly observed due to the scavenging effect of the anions that scavenge hole (h+) and/or OH• and form ionic radicals such as Cl• and $CO_3\bullet^-$, thus radicals were less photo-oxidizing species than (h+) and OH• (Kamble *et al*., 2006; Eslamia *et al*., 2016). In conclusion, the adsorbed anions compete with organic contaminants for the photo-oxidizing species on the surface of catalyst and prevent the photocatalytic degradation of the organic dye (Chen *et al*., 2007).

4.2.1.7. Effect of Amine sorption-photocatalysis of MO and Real Sample

To study the influence of amine on the photocatalytic efficiency of Zr-MOF (UiO-66-DMF-HT) for decolorizing of Real sample, we synthesized amine-functionalized Zr-MOF. The degradation efficiency of both MOFs is depicted in Figure 19.

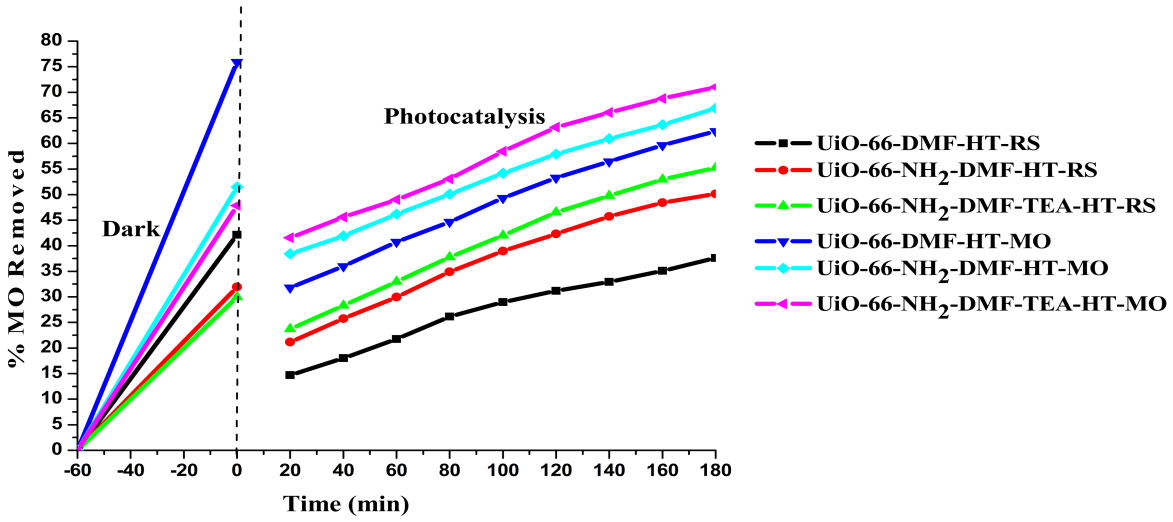

Figure 19.Effect of presence of amine on the degradation of MO and RS using equal 0.15g/L of selected photocatalysts under dark and visible light illumination.

In general, the presence of amine on zirconium MOFs improved the photocatalytic degradation of organic dye pollutants both for model pollutant and real sample situation. The higher efficiency exhibited by amine functionalized MOFs could be attributed to band gap modulation (Musho *et al*., 2014) and delay in e-h^+ recombination. The performance of the as-synthesized MOFs in general exhibited higher efficiency in both sorption and photocatalysis for a Model pollutant than real sample. Similar report has been made by Muluneh (2016) for iron based MOFs. Kiros *et al*. (2016) and Tedla *et al*., (2015) have also reported the same trend for zeolites supported TiO_2 and Zn-Fe-Mn Nanocomposites respectively. This can be as the result of additional pollutants with the target dye. When it comes to adsorption, Zr-MOF taken up more sorbet than the functionalized Zr-MOFs. This is possible due to the higher BET surface area of the former than the later (Table 5).

4.3. Point of Zero Charge of the selected Zr-MOF

The point of zero charge is a concept relating to the phenomenon of adsorption and it describes the condition when electrical charge density on surface is zero or neutral. The photocatalyst surface has a net positive charge at pH < pHPzc and a net negative charge at pH > pH_{PZC}. With this into account, we tried to determine the pH_{PZC} of the Zr-MOF exhibiting better catalytic efficiency with pH between 2.0 and 12.0, the result of which is shown in Figure 20. The pH_{PZC} of the photocatalyst was found to be 6.04, which is accepted to be the point at which the surface charge of the photocatalyst is zero. This shows that the synthesized photocatalyst surface of UiO-66-NH_2-TEA-HT has net positive charge (acidic properties) below 6.04, net negative charge (basic) above 6.04 and neutral at pH = 6.04.

The adsorption and photocatalysis processes are very less at pH_{PZC} due to the less interaction between the positive modified photocatalyst surface and anionic MO. Hence, the adsorption and photocatalysis of anionic dyes is favoured at pH values lower than the pH_{PZC} as witnessed in the result shown in Figure 20.

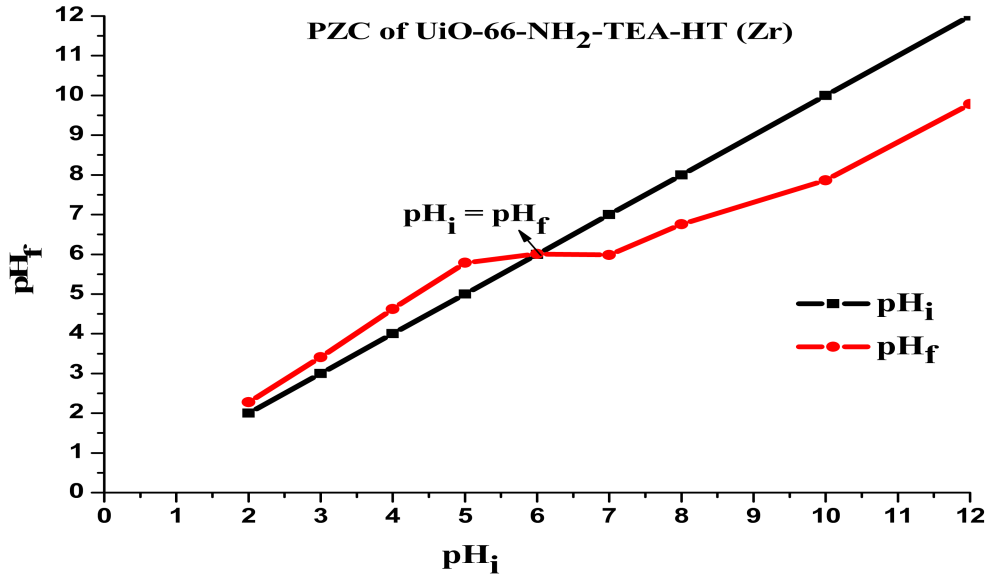

Figure 20. Plot of Point of Zero Charge of the photocatalyst, UiO-66-NH_2-TEA-HT (Zr)

4.4. Recycling of Photocatalysts

Recycling is a very important parameter to assess the practical application of photocatalysts in wastewater treatment. The reuse of photocatalysts contributes significantly to lessen the operational cost of photocatalyst. To test the reusability of the photocatalyst system for first run, 10ppm of MO and 0.15gL^{-1} of photocatalyst load adjusted at pH =4 were used.

In this work, the catalyst recycling test reaction was performed with recovered catalyst under the same conditions as that used in the first run. Here, the reused catalysts were washed twice with HPLC grade methanol and then centrifuged and dried after 15 minutes interval at 4000 rpm for each successive run (Shen *et al*., 2014). The same procedure was under gone for each cycle run. The percentage degradation of MO removed verses contact time was plotted for each recycling photocatalyst, (UiO-66-NH_2-TEA-HT (Zr)), under dark and visible light irradiation as shown in appendix Table 9 and Figure 21.

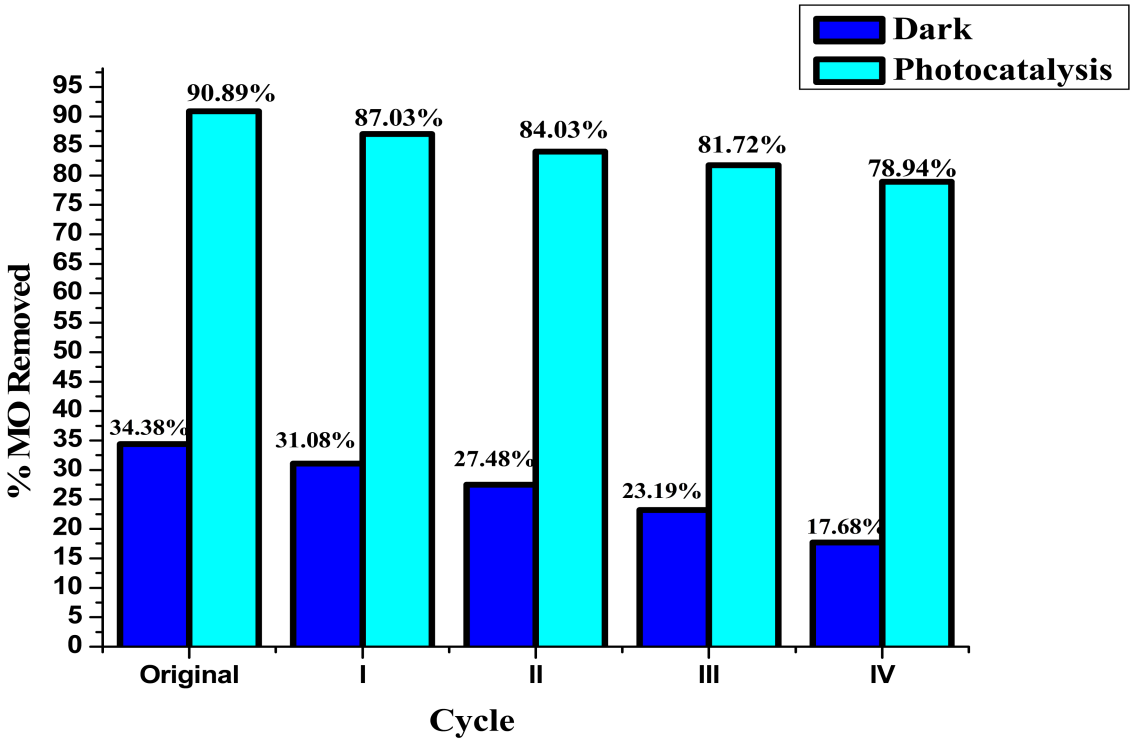

Figure 21. Recycling modified Zr-MOF photocatalyst for the degradation of MO under dark and visible light illumination

The experimental results revealed that the photocatalyst efficiency decreases with increased number of cycles. The degradation efficiencies of 90.89%, 87.03%, 84.03%, 81.72% and 78.94% were observed in cycles 0, I, II, III and IV respectively. Moreover, the dark adsorption

results of 34.38 %, 31.08 %, 27.48 %, 23.19 % and 17.68 % were achieved after original, I, II, III and IV recycles respectively. Hence, both dark adsorption (from 34.38% to 17.68%) and degradation efficiency (from 90.89% to 78.94%) decreased when the reusability of photocatalyst increased from original to cycle IV. This may be due to decreased active cites of the photocatalyst that causes prevention of the visible light penetration from striking the surface of the photocatalyst. The results show that the photocatalyst is basically stable and is promising for environmental remediation. As result, UiO-66-NH_2-TEA-HT could retain its activity fairly well even after four cycles of application indicating that the as-synthesized UiO-66-NH_2-TEA-HT MOF can be re-generated and re-used for reasonable times (Shen *et al*., 2014 ; Lin *et al*.,2015).

4.5. Real Sample Treatment under Visible Light

Real Sample of dyed textile wastewater from Awassa textile industry, Awassa, was decolorized using the modified effective photocatalyst, UiO-66-NH_2-TEA-HT (Zr), under optimized conditions and visible light irradiation. Then the plot of percent degradation of MO and percent degradation of real waste water sample versus irradiation time (in min) were plotted in Figure 22 and given in appendix Table 10.

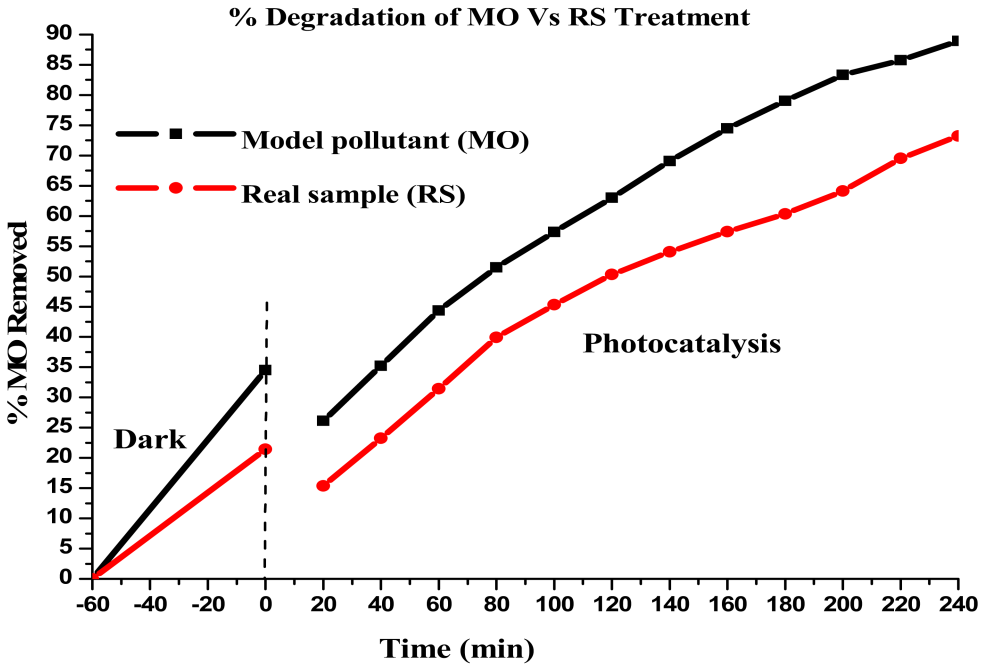

Figure 22. Plot of % Dye removal of model pollutant (MO) and real waste water sample under dark and visible light using UiO-66-NH_2-DMF-TEA-HT (Zr)(0.3M H_2O_2 concentration with parameters kept constant).

Figure 22 and appendix Table 10 shows that the adsorption of the model pollutant (MO) and the colored waste water samples at dark were 34.51% and 21.42% respectivelly. Moreover, the percentage degradation of the model pollutant (MO and the real waste water sample under visible light were 88.93% and 71.24% respectivelly. These expermental results show that the adsorption and percentage degradation of real waste water samples were lower than the adsorption as well as the percentage degradation of optimized model pollutant (MO). This is

may be due to the fact that textile waste water contains various type of dyes with various concentration. Besides the dyes composition could of anionic and cationic in nature that might influence the optimum setting obtained for a model pollutant. Further more, the higher concentration of different types of dyes in the real sample could reduce the degradation effecincy of UiO-66-NH_2-TEA-HT (Zr) due to the prevention of visible light from reaching the surface of the catalyst (Jing *et al*., 2014).

5. SUMMARY, CONCLUSIONS AND RECOMMENDATIONS

5.1. Summary and Conclusions

In this work, Zr-MOFs and their respective modified Zr-MOFs were successfully synthesised at room temperature with solvent DIW and at high temperature with DMF. For HT synthesis of Zr-MOFs, oven set at 120^0c and Pyrex glass bottles were used instead of Teflon-lined steel autoclave.

In addition, as-synthesized Zr-MOFs were characterized using FTIR, PL, UV-Vis, TGA, XRD, BET, and SEM. The FTIR results shown that the as-synthesised materials contain O-H, N-H and C-N bands. From UV-Vis, the effective modified photocatalyst shows the lower band gap energy. The PL marks the least optical intensity was observed for the effective photocatalysts. XRD results revealed that as-synthesized materials were Zr-MOFs. The XRD and BET results also showed that Zr-MOFs (UiO-66) have the smaller crystalline sizes compared to the

amine-functionalized Zr-MOFs. SEM micrograph showed irregular particles exhibited by the as-synthesized Zirconium MOFs.

As-synthesized Zr-MOFs (photocatalysts) were used to deliberate photocatalytic degradation of MO aqueous solution under visible light. The degradation efficiency of UiO-66-NH_2-DMF-TEA-HT was found to be higher at low dye concentration, optimum photocatalyst load and at pH=4 under visible light; this is due to its smaller particle size, delayed e-h^+ recombination and the smaller band gap energy (Eg) making it amenable for attracting more photons in the visible region. Moreover, amine-functionalized Zr-MOFs have better degradation efficiency than Zr-MOFs. In addition, UiO-66-NH_2-TEA-HT can be easily regenerated and re-used for several times, which show this photocatalyst could have large potential for the degradation of dye-containing wastewater. The removal of dyes from MO aqueous solution and real waste water sample using UiO-66-NH_2-DMF-TEA-HT under the optimized conditions were found to be 88.93% and 71.24%, respectively.

5.2. Recommendations

The following recommendations can be made as a result of the outcome of this study:

- Further research on the photocatalytic degradation of organic pollutants using MOFs will be taken for future work on effect of parameters such as: reaction mixing time, synthesis method, reaction temperature, light effect and light intensity.
- In order to achieve the effective degradation efficiency researchers should be studied the ternary nano systems of combining inorganic compounds with MOFs.
- Since there is a dearth of work on photocatalytic degradation efficiency of MOFs for the effective removal of organic dyes from not only the textile industry but also from other industries further researchers should be studied in this area.
- Further research on the adsorption and photocatalytic degradation of organic pollutants will be taken for future work on using other model pollutants such as Methylene blue (MB).

6. REFERENCES

Abdullah, M., Low, G. and Mathews, R. W. 1990. Effects of common inorganic ions on rat of photocatalytic oxidation of organic carbon over illuminated titanium dioxide. *Journal of Physical Chemistry*, 94: 6820.

Achmann, S., Hagen, G., Kita, J., Malkowsky, I., Kiener, C. and Moos, R. 2009. Metal organic frameworks for sensing applications in the gas phase. *Sensors*, 9: 1574-1589.

Adedibu, C.T. and Isaac, Y.A. 2012. Syntheses and applications of metal organic framework materials: *a review*. *Journal of Acta Chimica and Pharmaceutica*, *Indica,* 2 (2): 75-81.

Adeyemo, A.A., Adeoye, I.O. and Bello, O.S. 2012. Metal organic frameworks as adsorbent for dye adsorption: Overview of prospects and future challenges. *Journal of* Toxicolo*gical & Environmental Chemistry*, 94 (10): 1846–1863.

Agarwal, K. 2013. Removal of dyes using conventional and advanced adsorbents. A Project Report, National Institute of Technology Rourkela, Rourkela.

Akbal, F. and Onar, A.N. 2003. Photocatalytic degradation of phenol. *Journal of Environmental Monitoring and Assessment*, 83: 295–302.

Alemseged, E., Yadav, O.P., and Bachheti, R.K. 2013. Photocatalytic degradation of methyl orange dye using Cr-doped ZnS nanoparticles under visible radiation. *International Journal of Chemical Technology,* 5(4): 1452-1461.

Almansa, M.A. 2016. Post-functionalized Hybrid Materials as Multi-site Catalysts. Doctoral Dissertation, University of Spain, Madrid.

Andrew, D.W., Jong-San, C., Christian, S., Philip, L. and Llewellyn, L. 2013. An adsorbent performance Indicator as a first step evaluation of novel sorbents for gas separations: application to MOFs. *Langmuir*, 29: 3301-3309.

Bhatkhande, D.S., Pangarkar, V.G. and Beenackers, A.A. 2001. Photocatalytic Degradation for Environmental Applications. A review article, *Journal of Chemical technology,* 77(1):102–116

Cao J., B.D. Luo, H.L. Lin, B. Xu, S. Chen. 2012. Aluminium salt slag characterization and utilization. Review article, *Journal of Hazardous Materials*, (217–218): 1-458.

Chen, B. and Qian, G. 2014. Metal organic frameworks for photonics applications. Springer *Heidelberg New York Dordrecht London.*

Chen, C.C., Lu, C.S., Chung, Y. C., and Jan, J .L .2007. UV light induced photodegradation of malachite green on TiO_2 nanoparticles. *Journal of Hazardous Materials*, 141: 520–528.

Chen, Q., He, Q., Lv, M., Wei, F. 2015. Selective adsorption of cationic dyes by UiO-66 NH_2.*Article in Applied Surface Science*, 327: 85 .DOI:10.1016/j.apsusc.2014.11.103.

Chen, S., Zhang, J., Zhang, C. Yue, Q., Li, Y. and Li, C. 2010. Equilibrium and kinetic studies of methyl orange and methyl violet adsorption on activated carbon derived from phragmites Australia. *Desalinations*, 252: 149–156.

Chira, R., Bhattacharjee, D .and Abhijit, N. 2011. *Physical Science Technology,* (7): 122.

Chong, M.N., Jin, B., Chow, C.W. and Saint, C. 2010. Recent developments in photocatalytic water treatment technology: A review. *Journal of Water Resource*, 44: 2997–3027.

Colmenars, C.J. and Luque, R.2014. Heterogeneous photocatalytic nanomaterials: prospects and challenges in selective transformations of biomass-derived compounds**.** *Journal of Royal Society of Chemistry*, 43: 765-778.

Crini, G. 2006. Nonconventional low-cost adsorbents for dye removal: a review. *Journal of Biology and resource Technology*, 97: 1061–85

Du, J.J., Yu-Peng, Y., Jia-Xin, S., Fu-Min, P., Xia, J., Ling-Guang, Q. An-Jian, X., Yu-Hua, S. and Jua-Fu, Z. 2011. New photocatalysts based on MIL-53 metal-organic frameworks for the decolorization of methylene blue dye. *Journal of Hazardous Materials,* 190 (1-3): 945-951.

Ece, O. 2012. Hydrothermal Synthesis and Structural Characterization of Open-Framework Metal Phosphates Templated With Organic Diamines. (Unpublished MSc thesis), *Journal of Izmir Institute of Technology.*

Eslamia, A., Aminib, M.M., Yazdanbakhsh, A.R., Mohseni-Bandpeic, A., Safarid, A.A. and Asadi, A. 2016. N, S-Co-Doped TiO2 Nanoparticles and Nanosheets in Simulated Solar Light for Photocatalytic Degradation of Non-Steroidal Anti-Inflammatory Drugs in Water: A Comparative Study. *Journal of Chemical technology Biotech no*: doi:10.1002/jctb.4877.

Francesc, X., Avelino, C. and Hermenegildo, G. 2007. Applications for metal organic frameworks as quantum dot semiconductors. *Journal of American Chemical Society*, 111: 80-85.

Furukawa, H., Cordova. E.K., Keeffe, O.M., and Yaghi, M.O. 2013. The Chemistry and Applications of Metal-Organic Frameworks DOI: 10.1126/science.1230444, *Science V.341*

Gu, Z. 2014. Synthesis and characterization of surface mounted chiral metal organic frameworks. Doctoral Dissertation, Karlsruhe Institute of Technology, genehmigte.

Habeeb, A.H., and Hussein, S.B. 2016. Optimization of degradation of Trypan Blue Dye using Advanced Oxidation Processes and Photocatalysis under UV Light. (Unpublished MSc Thesis), University of Al-Qadisiya.

Haileyesus,Tedla. Isabel, Díaz.Tesfahun, Kebede.and Abi, Taddesse.M.2015.Synthesis, characterization and photocatalytic activity of zeolites supported ZnO/Fe_2O_3/MnO_2 nan o composites. *Journal of Environmental Chemical Engineering*, (3):1586–1591.

Haque, E., Lee, J.E., Jang, I.T., Hwang, Y.K, Chang, J.S., Jegal, J. and Jhung, S.H. 2010. Adsorptive removal of methyl orange from aqueous solution with MOFs, porous chromium benzenedicarboxylates. *Journal of Hazardous Materials*, 181: 535-542.

Hamoudi, S., El-Nemr, A., and Belkacemi, K. 2010. Adsorptive removal of di hydrogen phosphate ion from aqueous solutions using mono, di- and tri ammonium-functionalized SBA-15. *Journal of Colloid Interface Science*, 343: 615-621

Hasan, Z., Cho, W-D., Nam, I-H., Chon, C-M., and Song, H. 2016. Preparation of Calcined Zirconium-Carbon Composite from Metal Organic Frameworks and Its Application to Adsorption of Crystal Violet and Salicylic Acid, *Journal of Hazardous Materials*, 9:261; doi:10.3390/ma9040261.

Hayes, G.R., and Deveaud, B. 2002. "Is Luminescence from Quantum Wells Due to Excitons, *Journal of physical status solid, 190* (3): 637–640.

Hernandez-Alonso, D.M., Fresno, F., Suarez, SJ.M. and Coronado, M.SJ. 2009. Development of alternative photocatalysts to TiO_2: challenges and opportunities, *Energy Environmental Science*, 2: 1231–1257.

Herrmann, J.M. 1999**.** Heterogeneous photocatalysis: fundamentals and applications to the removal of various types of aqueous pollutants. *Journal of Catalysis Today*, 53 (1): 115-129.

Hinterholzinger, F.M. 2013. Metal-organic frameworks for chemical sensing applications. (Unpublished Ph.D. dissertation).

Hoffmann, M.R., Martin, S.T., Choi, W. and Bahnemann, D.W. 1995. Environmental applications of semiconductor photocatalysis. *Chemical Review,* 95 (1): 69-96.

Holliday, G. and Smith, A. 2014. Design and application of metal organic frameworks containing Porphyrin Photosensitizers, (Unpublished qualifying project Report), *Worcester Polytechnic Institute*.

Houa, J., Luana.Y, Tanga.J, Wensleya, M.A., Yanga, M, Lub, Y.2015. Synthesis of UiO-66-NH_2 derived heterogeneous copper (II) catalyst and study of its application in the selective aerobic oxidation of alcohols. *Journal of Molecular Catalysis A,* 407:53–59

James, L.S., Pichon, A. and Lazuen-Garay, A. 2006. Solvent free synthesis of a microporous metal organic framework. *Journal of Crystal Engineering Community, 8*: 211-214.

Jiao, G., Jin, Y., Ying-Ying, L. and Jian-Fang, M. 2012. Two novel 3D metal–organic frameworks based on two tetrahedral ligands: syntheses, structures, photoluminescence and photocatalytic properties. *Journal of Royal Society of Chemistry*, 14: 6609-6617.

Jiang, B., Zheng, J., Liu, Q. and Wu, M. 2012. Degradation of azo dye using non-thermal plasma advanced oxidation process a circulatory airtight reactor system. *Chemica*l *Engineering Journal*, 204–206: 32–39.

Jing, H.P., Wang, C.C., Zhang, Y.W., Wang, P. and Li, R. 2014. Photocatalytic degradation of methylene blue in ZIF-8. *Journal of the Royal Society of Chemistry*, 4: 54454-54462.

Kamble, S.P., Sawant, S.B. and Pangarkar, V.G. 2006. Photocatalytic Degradation of m-Dinitrobenzene by Illuminated TiO_2 in Slurry Photoreactor. *Journal of the Chemical and biological technology*, 81(3):365–373.

Kandiah, M. S., Usseglio, S., Svelle, U. Olsbye, K.P. and Tilset, S. 2010. Post-synthetic modification of the metal-organic framework compound UiO-66. *Journal of the Material Chemistry*, 20:9848-9851

Ke, F. L., Qiu, Y.-P., Yuan, F.-M. Peng, X. Jiang, A.-J. Xie, Y. Zhu. 2011. Thiol functionalization of metal-organic framework by a facile coordination based post synthetic strategy and enhanced removal of Hg_2 þ from water, *A Review. Journal of Hazardous Materials,* 196: 36-43.

Khan, N.A., Hasan, Z. and Jhung, S.H. 2012. Adsorptive removal of hazardous materials using metal-organic frameworks (MOFs): *A Review. Journal of Hazardous Materials,* 244-245: 444-456.

Khan, N.A., Jung, B.K., Hasan, Z., Jhung, S.H. 2015. Adsorption and removal of pathalic acid and diethyl phthalate from water with zeolitic imidazolate and metal organic frameworks. *Journal of Hazardous Material*, 282: 194-200.

Kiros, Guesh. Alvaro, Mayoral. Carlos, M.arquez. Alvarez.Yonas, Chebude. And Isabel, Diaz. 2016. Enhanced photocatalytic activity of TiO_2 supported on zeolites tested in real wast e waters from the textile industry of Ethiopia. *Journal of Microporous and Mesoporous Materials,* (225): 88-97.

Klug, P.H., Alexander, E.L. 1974. X-ray Diffraction Procedures for Polycrystalline and Amorphous Material, Second Edition, Wiley, New York.

Konstantinou, I. and Albanis, T. 2004."TiO2-assisted photocatalytic degradation of azo dyes in aqueous solution: kinetic and mechanistic investigations": A *Review. Applied Catalysis B: Environmental*, 49: 1–14.

Kuppler, R.J., Timmons, D.J., Fang, Q.R., Li, J.R., Makal, T.A., Young, M.D., Yuan, D., Zhao, D., Zhuang, W., Zhou, H.C. 2009. Potential applications of metal-organic frameworks: Review. *Coordination Chemistry Reviews,* 25: 3042–3066.

Laurier, K, G.M., Vermoortele, F., Ameloot, R., De Vos, D.E., Hofkens, J. and Roeaers, M.B.J. 2013. Iron (III)-based metal organic frameworks as visible light photocatalysts. *Journal of American Chemical Society*, DOI:org/10.1021/ja405086e.

Laurier, K, G.M., Eduard, F., Pedro, A., Koen, K., Hermenegildo, G., Mark, V.W., Dirk, E.D., Johan, H. And Maarten, B.J. 2014. Delayed electron-hole pair recombination in iron (III)- oxo metal organic frameworks. *Journal of Physical Chemistry*, 16: 5044-5047.

Li, L.J., Z. Rao., G.W., Song, B. Hu. 2013. Metal organic framework $[Cu_3 (BTC)_2 (H_2O)_3]$ for the adsorption of methylene blue from aqueous solution, *Desalination Water Treatment*. 18: 1-7.

Liu, W., Minglian, Wang, Chunxiang, Xu, Shifu .and Xianliang,F, F, F, Fu. 2013. $Ag_3 PO_4$/ZnO An efficient visible light sensitized composites with its application in photocatalytic degradation of Rhodamine *B. Materials. Research Bulletin.*48:106-113.

Lin, K.A., Chen, S.Y., and Jochems.P.A. 2015. Zirconium-based metal organic frameworks: Highly selective adsorbents for removal of phosphate from water and urine. *Journal of Chemistry and Physics*, 160: 168-176.

Lin, K.S., Adhikari, A.K., Su, Y.H., Chiang, C.L. and Dehvari, K. 2012. Structural characterization of chromium atoms in MIL-101 metal organic framework using XANES/EXAFS spectroscopy. *Chinese Journal of Physics, 50 (2): 322-331.*

Lin, K.Y.A. and Chang, H.A. 2015. Ultra-high adsorption capacity of zeolitic imidazole framework-67 (ZIF-67) for removal of malachite green from water. *Chemosphere,* 139: 624-631.

Lin, K.-Y. A., Liu, Y. T., and Chen, S. Y. 2016. Adsorption of fluoride to UiO-66-NH_2 in water: Stability, kinetic, isotherm and thermodynamic studies. *Journal of Colloid Interface Science*, 461: 79−87.

Long, J.,Wang,S.,Ding,Z.,Wang,S.,Zhou,Y.,Huang,L.andWang,,X. 2012. Amine functionalized zirconium metal–organic framework as efficient visible-light photocatalyst for aerobic organic transformations. *Journal of the Royal Society of Chemistry,* 48*:* 11656–11658.

Long, J.R., Dinca, M. and Yu, A.F. J.R. 2006. Microporous metal−organic framework incorporating 1, 4-benzeneditetrazolate: Syntheses, structures, and hydrogen storage properties. *Journal of American Chemical Society,* 128: 8904–8913.

Luu.L.C, Nguyen.V.T, Nguyen.T and Hoang.C.T. 2015. A Synthesis, characterization and adsorption ability of UiO-66-NH_2 .HYPERLINK "/2043-6262"2; *Advances in Natural Sciences Nanoscience and Nanotechnology*, V- 6:2

Ma, M. 2011. Prepartion and characterstics of MOFs for biological application. Doctoral Dissertation, University of Bochu.

Ma, S. and Meng, L. 2011. Energy-related applications of functional porous metal–organic frameworks. *Journal of Pure Applied Chemistry*, 83(1): 167–188.

Ma, S. and Zhou, H.C. 2010. Gas storage in porous metal–organic frameworks for clean energy applications. *Journal of the Royal Society of Chemistry*, 46: 44–53.

Mahalakshmi, M., Priya S.V., Arabindoo, B., Palanichamy, M. and Murugesan, V. 2009. Photocatalytic degradation of aqueous propoxur solution using TiO_2 and Zeolite supported TiO_2. *Journal of Hazardous Materials*, 161: 336 –343.

Manuel, S.S., Negash Getachew, Kenya, D., Manuel, D.G., Yonas, Chabude. And Isabel, D., 2014. Synthesis of metal organic frameworks in water at room temperature: salts as linker sources. *Journal of Royal Society of Chemistry, Green Chemistry,* DOI: 10.1039/c4gc01861c.

Mikaela, G. 2012. Metal organic frameworks for heterogeneous catalysis: synthesis and characterization. Dissertation*, Stockholm University, Sweden.*

Mittal, A., Malviya, A., Kaur, D., Mittal, J. and Kurup, L. 2007. Studies on the adsorption kinetics and isotherms for the removal and recovery of methyl orange from wastewaters using waste materials. *Journal of Hazardous Materials,* 148: 229–240.

Mohamed, E.F., 2011. Removal of organic compounds from water by adsorption and photocatalytic oxidation*. Doctoral Dissertation. Paris, France.*

Mohanty, R.P. 2012. Fabrication and characterization of metal organic framework based membrane. Doctoral *Dissertation, National Institute of Technology, Rourkela*.

Muluneh Endashaw. 2016. Synthesis and characterization of selected metal organic frameworks for photocatalytic degradation of methyl orange (Unpublished MSc thesis), Haramaya University, Haramaya, Ethiopia.

Musho, T., Li, J. and Nianqiang Wu, N.2014. Band gap modulation of functionalized metal organic frameworks**.** *Journal of Physical Chemistry,* 16:23645-2382

Negash Getachew, Yonas Chebude, Isabel, D. and Manuel, S.S. 2014. Room temperature synthesis of metal organic framework MOF-2. *Journal of Porous Materials, Springer*, 1 (5): 769-773.

Negash Getachew. 2013. Benign methods for the synthesis of metal organic frameworks. (Unpublished Doctoral Dissertation), Addis Ababa University, Addis Ababa, Ethiopia.

Nguyen, G.J., Cohen, M.S. 2010. *Journal of American Chemical society*, 132: 4560–4561

Parent, Y., Blake, D., Magrini, B. K., Lyons, C., Turchi, A., Watt, E., Wolfram, and

Praire.M.1996. Solar photo catalytic process for the purification of water: State of

development and barriers to commercialization. *Solar Energy*, 56: 429-437.

Pelizzetti, E. 1985. Homogeneous and heterogeneous photocatalysis. Reidel Publishing Company. Dordrecht, Holland.

Pham, M.H. 2013. Nanoscale metal organic frameworks: synthesis and application of bimodal micro-meso-structure and nanocrystals with controlled size and shape. *(*Unpublished thesis*), University Laval, Québec, Canada.*

Pujara, K., Kamble, S.P. and Pangarkar, V.G. 2007. Photocatalytic degradation of phenol-4 sulfuric acid using an artificial UV/TiO_2 system in slurry bubble column reactor. *Industrial Engineering Chemical Resource*, 46(12): 4257–4264

Rashed, M.N. and El-Amin, A.A. 2007. Photocatalytic degradation of methyl orange in aqueous TiO_2 under different solar irradiation sources. *International Journal of Physical Sciences,* 2 (3): 073-081.

Sadri, M.B. 2010. Degradation of methyl orange using ultrasonic irradiation: enhanced with adsorption using newspaper. (Unpublished MSc Thesis), University of Malaysia Pahang.

Samar, M. 2015**.** Photocatalytic Degradation of Organic Compounds in Water using Nanoparticle Thin Film. (Unpublished MSc Thesis), University of Al-Azhar Gaza.

Schroder, M. 2010. Functional metal-organic frameworks: gas storage, separation and catalysis. *Springer Heidelberg,* 293.

Shankar, M.V., Anandan, S., Venkatachalam, N., Arabindoo, B. and Murugesan, V. 2004. Novel thin-film reactor for photocatalytic degradation of pesticides in aqueous solutions. *Journal of Chemical Technology and Biotechnology,* 79: 1279–1285.

Shen, L., Liang, R., Luo, M*.,* Jing, F. and Wu, L.2014. Electronic effects of ligand substitution on metal organic frameworks photocatalysts: The case study of UiO-66. *Journal of Photocatalysis on Energy and Environment,* 117-118: 326-458.

Shetty, R., Kothori, G., Tambe, A.S., Kulkarni, D.B. and Kamble, P.S. 2016. Photocatalytic degradation of ciprofloxacin, HCl using P-25 TiO_2 photocatalyst: Comparative evaluation of solar and artificial radiation. *Journal of chemistry*, 55:16-22

Silva, G.C. Luz, I., Francesc X., Corma, A. and Garcia, H. 2010. Water stable zirconium benzenedicarboxylate metal organic frameworks as photocatalysts for hydrogen generation. *Journal of European,* 16: 11133-11138.

Sobczynski, A., Duczmal, L. and Zmudzinski, W. 2004. Phenol destruction by photocatalysis on TiO_2: an attempt to solve the reaction mechanism. *Journal of Molecular Catalysis,* 213: 225–230.

Stock, N. and Biswas, S. 2012**.** Synthesis of metal organic frameworks: routes to various MOF morphologies and composites*.* *Chemical Reviews,* 112 *(2)*: 933-969.

Susumu, K., and Joe, H.C. 2014. Metal–Organic Frameworks (MOFs) .*Journal of Hazardous Materials,* 48: 219–220.

Tanabe, K. K., and Cohen, S. M. 2011.*Chemical Society Review, 40*: 498-519

Tsai, W.T., T.Y., Su, K.Y., and T, H. Dai. 2007. The Adsorption of Cationic Dye from Aqueous Solution onto Acid-activated Andesite: *Journal of Hazardous Materials,* 1473:1056–1062.

Tsai, F.Ch. Xia, Y., Ma, N., Shi, J.J., Jiang, T., Chiang, T.Ch., Zhang, Z-C., Tsen, W.Ch.2014. Adsorptive removal of acid orange 7 from aqueous solution with metal– organic framework material, iron (III) trimesate. *Desalination and Water Treatment,* 57(7):3218- 3226.

Tsegaye, 2017. Synthesis and characterization of UiO-66 metal organic frameworks for simultaneous sorption of methyl orange and methylene blue from aqueous solution (Unpublished Msc Thesis), Haramaya University, Haramaya

Tuschel, D. 2016. Photoluminescence Spectroscopy Using a Raman Spectrometer. *Spectroscopy*, V, 31, Issue 9: 14–21

Vakiti, R.J. 2012. Hydro/solvothermal synthesis, structures and properties of metal organic frameworks based on S-block metals. Masters thesis and specialist projects*.* *Journal of Bowling Green, Kentucky University,* paper 1168.

Vellingiri, K., Boukhvalovb, W.D., Pandeyc, K.S., Deepd, A, and Kima.K-H. 2017. Luminescent metal-organic frameworks for the detection of nitrobenzene in aqueous media. *Journal of chemical Sensors and Actuators B*, 245: 305–313.

Wang, Z. Q., Cohen, S. M.2009.*A Review of Chemical Society, 38*: 1315

Wang. C.C., Li.R-J, Zhangc.Q-Y and Guo.G, 2014. Photo catalytic organic pollutants degradation in metal–organic frameworks. DOI: 10.1039/c4cs00003j

Wilkinson, G., Gillard, R.D. and McCleverty, J. A. 1987. The synthesis, reactions, properties and applications of coordination compounds of late transition *e*lements. First edition, volume 5, Oxford: Pergamon Press.

Yaghi, O. M. and Li, H.L .1995. Hydrothermal synthesis of a metal organic framework containing large rectangular channels. *Journal of American Chemical Society,* 117 (41): 10401–10402.

Zhang, Z., Wang, C.C., Zakaria, R. and Ying, J.Y. 1998. Role of particle size in nano crystalline TiO_2 based photocatalysts. *Journal of Physical Chemistry,* 102: 10871-10878.

Zhu, C., Wang, L., Kong, L., Yang, X., Zheng, S., Chen, F., Maizhi, F. and Zong, H. 2000. Photocatalytic degradation of azo dyes by supported TiO_2/UV in aqueous solution. *Chemosphere,* 41: 303–309.

7. APPENDICES

7. 1.Appendix Tables

Appendix Table 1. Percentage degradation of MO dye as a function of time under visible irradiation using different as-synthesized photocatalyst (photocatalyst load=0.15gL^{-1} and initial dye of 10ppm).

Time	Z_1	A_1	Z_2	A_2	A_3	Z_3	A_4	Z_4
-60	0	0	0	0	0	0	0	0
0	38.64	16.21	78.24	48.24	22.78	27.38	37.02	40.71
20	13.78	17.23	11.92	18.01	12.72	13.55	14.03	12.94
40	23.01	29.21	12.08	22.76	24.32	17.31	21.58	14.98
60	24.98	36.98	13.01	29.01	40.02	21.02	24.26	16.01
80	25.92	40.12	14.06	33.31	48.02	27.76	28.41	18.94
100	27.02	43.82	15.78	35.24	51.72	30.33	31.08	20.21
120	28.01	46.79	16.97	44.21	53.68	33.29	37.14	22.74
140	31.28	48.21	17.34	45.68	54.31	36.98	40.96	25.76
160	33.72	52.76	19.21	46.64	56.72	39.73	43.04	26.32
180	40.02	54.38	19.86	49.03	58.92	43.32	47.23	28.03

Appendix Table 2. Effect of pH on the degradation of MO using modified Zr-MO photocatalysts under dark and visible light illumination (Photocatalyst load=0.15gL^{-1} and 10ppm of MO).

Time(min)	pH=2	pH=4	pH=6	pH=8	pH=10	pH=12
-60	0	0	0	0	0	0
0	12.46	29.46	24.21	14.46	7.24	5.92
20	5.24	19.38	14.28	7.24	3.82	1.98
40	16.16	28.43	23.23	13.16	11.68	7.72
60	21.86	37.12	32.43	19.86	16.42	11.38
80	27.42	43.38	39.12	24.42	21.32	16.74
100	31.68	49.23	43.38	29.68	26.41	21.42
120	37.26	55.94	47.89	33.26	30.28	25.86
140	40.61	61.09	53.78	39.61	35.12	26.78
160	46.51	66.67	60.45	44.51	38.23	29.34
180	50.22	71.92	66.29	49.22	43.56	33.04

A

Appendix Table 3. Effect of photocatalyst load on the degradation of MO using modified Zr-MOF photocatalysts under dark and visible light illumination (MO of 10ppm with Ph adjustment at 4).

Time	0.05gL^{-1}	0.1gL^{-1}	0.15gL^{-1}	0.2gL^{-1}	0.25gL^{-1}	0.3gL^{-1}
-60	0	0	0	0	0	0
0	12.82	18.95	31.38	27.28	23.21	15.24
20	7.24	16.21	29.46	24.21	19.01	11.46
40	11.68	21.34	35.43	31.23	24.98	16.16
60	16.42	27.64	40.12	36.43	33.03	21.86
80	21.32	31.23	44.38	40.12	37.07	27.42
100	26.41	37.12	50.23	44.38	41.44	31.68
120	30.28	41.21	57.94	49.89	46.94	37.26
140	35.12	47.66	62.09	54.89	51.97	40.61
160	38.23	53.42	66.67	61.45	56.58	46.51
180	43.56	57.89	72.69	67.29	63.59	50.22

Appendix Table 4. Effect of initial dye concentration on the degradation of MO using modified Zr-MOF photocatalyst under dark and visible light illumination (photocatalyst load=0.15gL^{-1} with pH adjustment at 4).

Time(min)	10ppm	15ppm	20ppm	25ppm	30ppm	35ppm
-60	0	0	0	0	0	0
0	37.38	27.25	23.18	19.23	15.28	12.21
20	28.46	23.28	18.24	14.67	10.52	7.26
40	33.43	29.26	24.34	21.42	16.32	13.11
60	39.12	34.38	30.12	27.21	22.12	19.32
80	43.38	39.21	35.38	31.23	27.21	22.21
100	49.23	45.28	41.21	37.12	33.38	29.24
120	54.94	51.21	46.38	42.38	37.28	32.38
140	61.09	56.38	50.12	45.22	40.12	36.03
160	66.67	60.22	54.34	49.69	43.44	38.08
180	71.69	64.44	57.13	52.13	46.13	39.26

Appendix Table 5. Effect of electron acceptors (H_2O_2) on the degradation of MO using the amine-functionalized Zr-MOF under dark and visible light illumination (MO=10ppm, $0.15gL^{-1}$ photocatalyst and 0.1M-0.5M H_2O_2 with pH adjustment at 4).

Time	0M	0.1M	0.2M	0.3M	0.4M	0.5M
-60	0	0	0	0	0	0
0	32.38	39.41	45.56	51.38	48.18	44.74
20	13.46	18.61	26.83	35.61	29.98	23.28
40	22.43	27.48	35.01	43.78	38.38	31.92
60	33.12	36.88	42.93	50.05	46.15	40.16
80	37.38	41.76	47.91	56.74	51.13	44.92
100	44.23	48.23	54.88	61.75	58.12	51.44
120	49.94	53.88	59.86	67.09	63.11	56.64
140	54.09	57.53	65.14	71.12	68.43	61.14
160	55.67	59.75	67.78	74.81	70.42	63.23
180	56.68	64.82	72.05	78.17	73.08	65.98

Appendix Table 6. Mechanism of photocatalytic degradation of MO using the modified Zr-MOF under dark and visible light illumination (MO= 10ppm, $0.15gL^{-1}$ photocatalyst and $100mgL^{-1}$ of $NaHCO_3$, CH_3OH and $AgNO_3$ with pH adjustment at 4).

Time	Without scavenger	$0.1gL^{-1}$ $NaHCO_3$	$0.1gL^{-1}$ CH_3OH	$0.1gL^{-1}$ $AgNO_3$	Time	Without scavenger	$0.1gL^{-1}$ $NaHCO_3$	$0.1gL^{-1}$ CH_3OH	$0.1gL^{-1}$ $AgNO_3$
-60	0	0	0	0	100	39.14	20.98	35.29	29.16
0	28.46	18.38	10.68	14.28	120	46.43	26.72	40.98	33.68
20	13.23	3.88	9.82	7.92	140	52.33	31.82	47.23	39.74
40	19.51	8.32	15.74	11.52	160	59.14	37.67	52.92	44.82
60	26.14	12.38	22.86	17.54	180	65.24	41.32	58.08	50.01
80	33.48	17.12	29.73	24.32					

Appendix Table 7.Effect of co-existing ions on the degradation of MO using the modified Zr-MOF under dark and visible light illumination (MO= 10ppm, $0.15gL^{-1}$ photocatalyst, $0.5gL^{-1}$ of Na_2CO_3 and NaCl with pH adjustment at 4).

Time	Without anion	$0.5gL^{-1}$ Na_2CO_3	$0.5gL^{-1}$ NaCl	Time	Without anion	$0.5gL^{-1}$ Na_2CO_3	$0.5\ gL^{-1}$ NaCl
-60	0	0	0	100	42.14	22.98	33.29

0	28.46	21.38	12.68	120	47.43	27.72	37.98
20	14.23	2.88	7.82	140	53.33	32.82	43.23
40	22.51	7.32	14.74	160	59.14	37.67	48.90
60	29.14	12.38	21.86	180	66.64	42.32	52.08
80	36.48	17.12	28.73				

Appendix Table 8. Effect of Amine sorption-photocatalysis of MO and Real Sample using the Zr-MOFs under dark and visible light illumination (MO=10ppm, 0.15gL^{-1} photocatalyst with pH adjustment at 4).

Time(min)	UiO-66-DMF-HT--RS	UiO-66-NH_2-DMF-HT-RS	UiO-66-NH_2-TEA-DMF-HT-RS	UiO-66-DMF-HT-MO	UiO-66-NH_2-DMF-HT-MO	UiO-66-NH_2-TEA-DMF-HT-MO
-60	0	0	0	0	0	0
0	42.15	31.92	29.95	75.93	51.47	47.83
20	15.67	21.16	23.72	33.81	38.42	41.54
40	19.01	25.72	29.32	36.98	41.92	44.61
60	21.74	29.96	32.98	40.74	46.16	49.01
80	24.13	34.91	37.76	45.67	49.08	53.07
100	25.98	37.94	42.01	49.32	53.15	58.46
120	28.18	43.33	46.52	54.28	57.92	62.15
140	29.93	45.72	49.78	57.47	60.93	66.01
160	30.06	47.44	50.94	59.65	63.63	67.79
180	31.61	48.15	51.24	63.39	68.89	71.03

Appendix Table 9. Reusability of the amine-functionalized Zr-MOF photocatalyst for the degradation of MO under dark and visible light illumination (MO= 10ppm, 0.15gL^{-1} photocatalyst load with pH adjustment at 4).

Time	Original	Cycle I	Cycle II	Cycle III	Cycle IV
-60	0	0	0	0	0
0	34.38	31.08	27.48	23.19	17.68
20	23.58	21.32	19.42	17.24	15.78
40	41.78	39.78	37.28	35.84	33.94
60	46.51	43.51	41.51	39.72	41.67
80	50.98	50.01	47.98	45.68	49.09
100	57.38	56.34	54.32	55.26	52.86
120	63.57	62.57	60.37	59.08	59.05
140	68.41	67.92	65.34	63.98	63.54
160	74.11	72.74	70.08	69.04	67.89
180	79.32	76.32	74.32	72.05	71.76
200	83.58	82.96	79.38	76.37	74.56
220	88.68	85.32	81.38	78.73	77.74

240	90.89	87.03	84.04	81.70	78.94

Appendix Table 10. Plot of % degradation of RS and MO using the modified Zr-MOFs under dark and visible light illumination (MO=10ppm, 0.3M H_2O_2 and 0.15gL^{-1} photocatalyst load with pH adjustment at 4).

Time	%MO Removal	Time	%MO Removal	Time	%RS Removal	Time	%RS Removal
-60	0	120	62.99	-60	0	120	50.31
0	34.51	140	69.08	0	21.42	140	54.05
20	23.13	160	74.47	20	15.38	160	57.43
40	31.22	180	79.02	40	23.24	180	60.34
60	44.38	200	83.32	60	31.41	200	64.13
80	51.47	220	85.78	80	39.92	220	69.51
100	57.34	240	88.93	100	45.34	240	71.24